Electronic Supplementary Material (ESI) for Chemical Science.
This journal is © The Royal Society of Chemistry 2022

Electronic Supplementary Information

Helicity-driven chiral self-sorting supramolecular polymerization with Ag^+: right- and left-helical aggregates

Mirae Ok[a,e], Ka Young Kim,[a,e], Heekyoung Choi[a], Seonghan Kim[b,c], Shim Sung Lee,[a] Jaeheung Cho*[b], Sung Ho Jung*[d] and Jong Hwa Jung*[a]

[a] *Department of Chemistry and Research Institute of Natural Sciences Gyeongsang National University, Jinju 52828, Korea*

[b] *Department of Chemistry, Ulsan National Institute of Science and Technology, Ulsan 44919, Korea*

[c] *Department of Emerging Materials Science, Daegu Gyeongbuk Institute of Science and Technology, Daegu 42988, Korea*

[d] *Department of Liberal Arts, Gyeongsang National University, Jinju 52828, Korea*

[e] *These authors are contributed equally.*

Contents

1. Method

2. Synthesis and characterization

3. Supplementary scheme and figures

4. Analytical data

Supplementary data

1. Methods

1.1 General characterization: The ^{1}H and ^{13}C NMR spectra were taken on a Bruker DRX 300, and Bruker DRX 500. Mass spectroscopy samples were analyzed on a JEOL JMS-700 mass spectrometer. The high resolution mass spectra (HR-MS) were measured by electrospray ionization (ESI) with a micro TOF Focus spectrometer from SYNAPT G2 (Waters, U.K.). A UV-visible spectrophotometer (JASCO J-815) was used to obtain the absorption spectra. IR spectra were observed over the range 500-4000 cm^{-1}, with a Thermo scientific Nicolet iS 10 instrument. Powder X-ray pattern (PXRD) was recorded on a Rigaku model NANOPIX X-ray diffractometer with a Cu K$_\alpha$ radiation source.

1.2 AFM observation: Atomic force microscope (AFM) imaging was performed by using XE-100 and a PPP-NCHR 10 M cantilever (Park systems). The AFM samples were prepared by spin-coating (2000 rpm) onto freshly cleaved Muscovite Mica, and images were recorded with the AFM operating in noncontact mode in air at RT with resolution of 1024 × 1024 pixels, using moderate scan rates (0.3 Hz). AFM images were recorded for fibers obtained from different ratio of right- and left-handed helix at diverse Ag$^+$ equivalents. In each image, 50~100 fibers were selected from different regions of the mica and analyzed using XEI software developed by Park systems.

1.3 Circular dichroism (CD) and UV-vis studies: The CD and UV-vis spectra were recorded on a Jasco J-815 CD spectrophotometer. The CD and UV-vis spectra were determined over the range of 200-500 nm using a quartz cell with 0.1 mm path length. Scans were taken at rate of 200 nm/min with a sampling interval of 0.5 nm and response time of 0.5 s. To elucidate the supramolecular polymerization process, we first prepared the sample by dissolving *R*-**L^1** (7.2 mM) with or without AgNO$_3$ in H$_2$O/DMSO (1:1 v/v). After adding the sample to the CD and UV cells, it was heated to 90 °C (1 °C/min) to form the monomeric species in CD and UV-vis spectroscopy. Then the sample was cooled to 20 °C (5 °C/min) in UV-vis spectroscopy. The time-dependent CD and UV-vis spectral changes were measured at 20 °C.

1.4 Calculation of thermodynamic parameter: The thermodynamic parameters governing the supramolecular aggregation of *R*-**L^1** were obtained by the global fitting of the melting curves. This global fitting is performed by using the equilibrium (EQ) model reported by ten Eikelder and coworkers.[1] The values for the elongation enthalpy (ΔH_e) and the entropy (ΔS_e), and elongation binding constant (K_e) used in the cooperative supramolecular polymerization models were determined by the global fitting of the heating curves,[2-4] which were obtained by plotting the degree of aggregation (α_{agg}) of *R*-**L¹** (7.0 mM) without and with $AgNO_3$ (1.2 equiv.) at 326 nm against temperature with heating experiments. An elongation binding constant (K_e) for aggregation at 293 K was estimated according to equation 1, from which the enthalpy change (ΔH), and the entropy change (ΔS) were determined:

$$K_e = e^{-(\Delta H_e - T\Delta S)/RT} \qquad \text{(equation 1)}$$

1.5 Preparation of silver complexes: Different concentrations (0~2.0 equiv.) of aqueous Ag^+ solution were added to *R*-**L¹** or *S*-**L¹** (6.4 mM) solution in DMSO/H_2O (1:1 v/v). Time- and temperature-dependent CD and UV-vis spectra were measured.

1.6 Calculation of stability constants: The UV-vis titration with $AgNO_3$ for *R*-**L¹** (50 μM) was performed in DMSO/H_2O (1:1 v/v). The titration was performed with 0-3.0 equiv. of $AgNO_3$ at 25 °C. Titration data were fitted into a desired binding model with HyperSpec to calculate stability constants for 1:1 and 2:1 (Ag^+ : ligand) complexes, respectively.[5-7]

1.7 Theoretical calculations: We performed density functional theory (DFT) calculations to optimize the Ag^+ complex systems using the Gaussian 09 package.[8] The unrestricted B3LYP functional was employed for all optimizations and frequency calculations with Def2-SVP level of theory for all atoms.[9-11] All calculations were performed in the gas phase. All the optimized structures were confirmed by vibrational frequency analysis with no imaginary frequency. The Cartesian coordinates are shown in Tables S2-S4.

2. Synthesis and characterization

2.1 Synthesis of *R*-L² and *S*-L²

(*R* or *S*)-(−)-2-amino-1-propanol (0.28 g, 3.7 mmol) was added to a stirred suspension of powdered KOH (1.05 g, 18.7 mmol) in dry DMSO (20 mL) at 60 °C. After 30 min, 4′-chloro-2,2′:6′,2″-terpyridine (1.00 g, 3.7 mmol) was added to the mixture. The mixture was then stirred for 4 h at 70 °C and poured into 600 mL of distilled water thereafter. CH_2Cl_2 (3 × 200 mL) was used to extract the aqueous phase. Residual water in dichloromethane was dried over Na_2SO_4 and CH_2Cl_2 was removed in vacuum, and the desired product was purified by recrystallization with ethyl acetate to give 0.72 g (72%) of *R*-**L²** and *S*-**L²**. Mp = 118.3 °C; IR (KBr pellet):

3375, 2964, 2926, 2846, 1577, 1565, 1473, 1439, 1403, 1353, 1204, 799 cm^{-1}; ^{1}H NMR (300 MHz, $CDCl_3$): δ 8.70 (tdd, *J* = 4.8, 1.8, 0.9 Hz, 2H), 8.62 (dt, *J* = 8.0, 1.1 Hz, 2H), 8.02 (s, 2H), 7.84 (td, *J* = 7.7, 1.8 Hz, 2H), 7.33 (ddd, *J* = 7.4, 4.8, 1.2 Hz, 2H), 4.14 (dd, *J* = 9.0, 4.1 Hz, 1H), 3.94 (dd, *J* = 9.1, 7.6 Hz, 1H), 3.41 (dddd, *J* = 10.6, 7.6, 6.6, 4.2 Hz, 1H), 1.21 (d, *J* = 6.5 Hz, 3H); ^{13}C NMR (125 MHz, DMSO-d_6): δ 167.2, 157.1, 155.3, 149.7, 137.9, 125.0, 121.3, 107.3, 75.1, 46.2, 20.43; HR-Mass (m/z) calculated for $C_{18}H_{18}N_4O$ $[M]^+$: 306.3690, Found $[M]^+$: 306.3690.

2.2 Synthesis of *R*-L^1

R-**L^1** and *S*-**L^1** was prepared according to a literature procedure.[12] In a two neck flask, *R*-**L^2** (0.50 g, 1.64 mmol) and TEA (0.1 mL, 0.72 mmol) were added to dry CH_2Cl_2 (10 mL). After cooling the solution in an ice bath, sebacoyl chloride (0.16 mL, 0.75 mmol) was added dropwise. The reactant was stirred for 3 h at room temperature. The crude product was recrystallized from CH_2Cl_2 to give a white crystalline solid *R*-**L^1** in 49.7% yield (0.632 g). Mp = 198 °C; IR (KBr pellet): 3428, 3311, 2929, 2845, 1640, 1582, 1563, 1466, 1446, 1407, 1362, 1207, 1038, 785 cm^{-1}; ^{1}H NMR (300 MHz, DMSO-d_6): δ 8.68 (m, 8H), 7.99 (m, 8H), 7.87 (d, *J* = 7.5 Hz, 2H), 7.50 (ddd, *J* = 7.7, 4.8, 1.6 Hz, 4H), 4.15 (m, 6H), 2.02 (t, *J* = 7.3 Hz, 4H), 1.42 (d, *J* = 7.5 Hz, 4H), 1.21 (s, 3H), 1.19 (s, 3H), 1.13 (s, 8H); ^{13}C NMR (125 MHz, DMSO-d_6): δ 172.3, 167.1, 157.2, 155.3, 149.7, 137.8, 125.0, 121.3, 107.2, 70.9, 44.1, 35.9, 29.2, 29.0, 25.7, 17.6; HR-Mass (m/z) calculated for $C_{46}H_{50}N_8O_4$ $[M]^+$: 778.3955, Found $[M]^+$: 778.3954.

2.3 Synthesis of *S*-L^1

The synthesis of *S*-**L^1** was performed as described in the synthesis of *R*-**L^1**. 52.4% yield (0.632 g). Mp = 198 °C; IR (KBr pellet): 3426, 3310, 2928, 2845, 1642, 1581, 1561, 1466, 1445, 1405, 1362, 1206, 1037, 786 cm^{-1}; ^{1}H NMR (300 MHz, DMSO-d_6): δ 8.70 (m, 8H), 7.95 (m, 8H), 7.86 (d, *J* = 7.4 Hz, 2H), 7.46 (ddd, *J* = 7.7, 4.7, 1.6 Hz, 4H), 4.17 (m, 6H), 2.12 (t, *J* = 7.2 Hz, 4H), 1.40 (d, *J* = 7.6 Hz, 4H), 1.19 (s, 3H), 1.17 (s, 3H), 1.11 (s, 8H); ^{13}C NMR (125 MHz, DMSO-d_6): δ 172.1, 167.0, 157.3, 155.0, 149.9, 137.6, 125.2, 121.5, 107.1, 70.8, 44.0, 35.7, 29.0, 28.8, 25.6, 17.5; HR-Mass (m/z) calculated for $C_{46}H_{50}N_8O_4$ $[M]^+$: 778.3955, Found $[M]^+$: 778.3953.

3. Supplementary scheme and figures

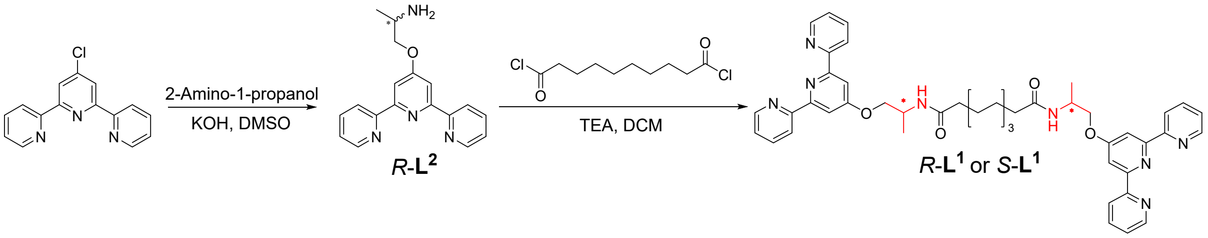

Scheme S1. Synthetic method of *R*-**L**^{1} or *S*-**L**^{1}.

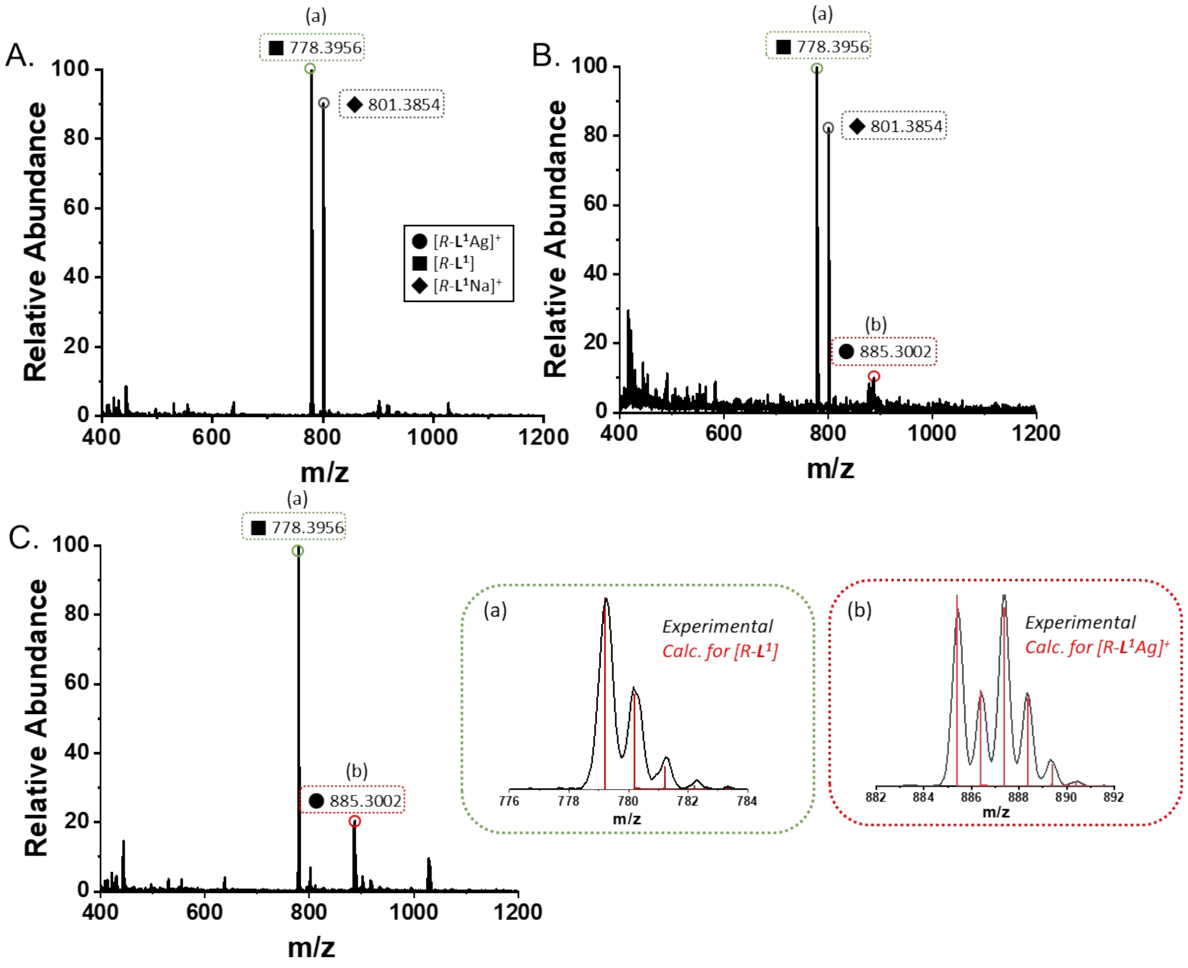

Fig. S1 HR-ESI-MS spectra of *R*-**L**^{1} (6.4 mM) in the presence of different equiv. of $AgNO_3$; (A) 0 equiv., (B) 0.1 equiv. and (C) 0.2 equiv. in DMSO/H_2O (1:1 v/v) after 72 h aging.

[*Note*] The peaks at m/z 801.3854 correspond to [*R*-**L**^{1}+Na]$^+$.

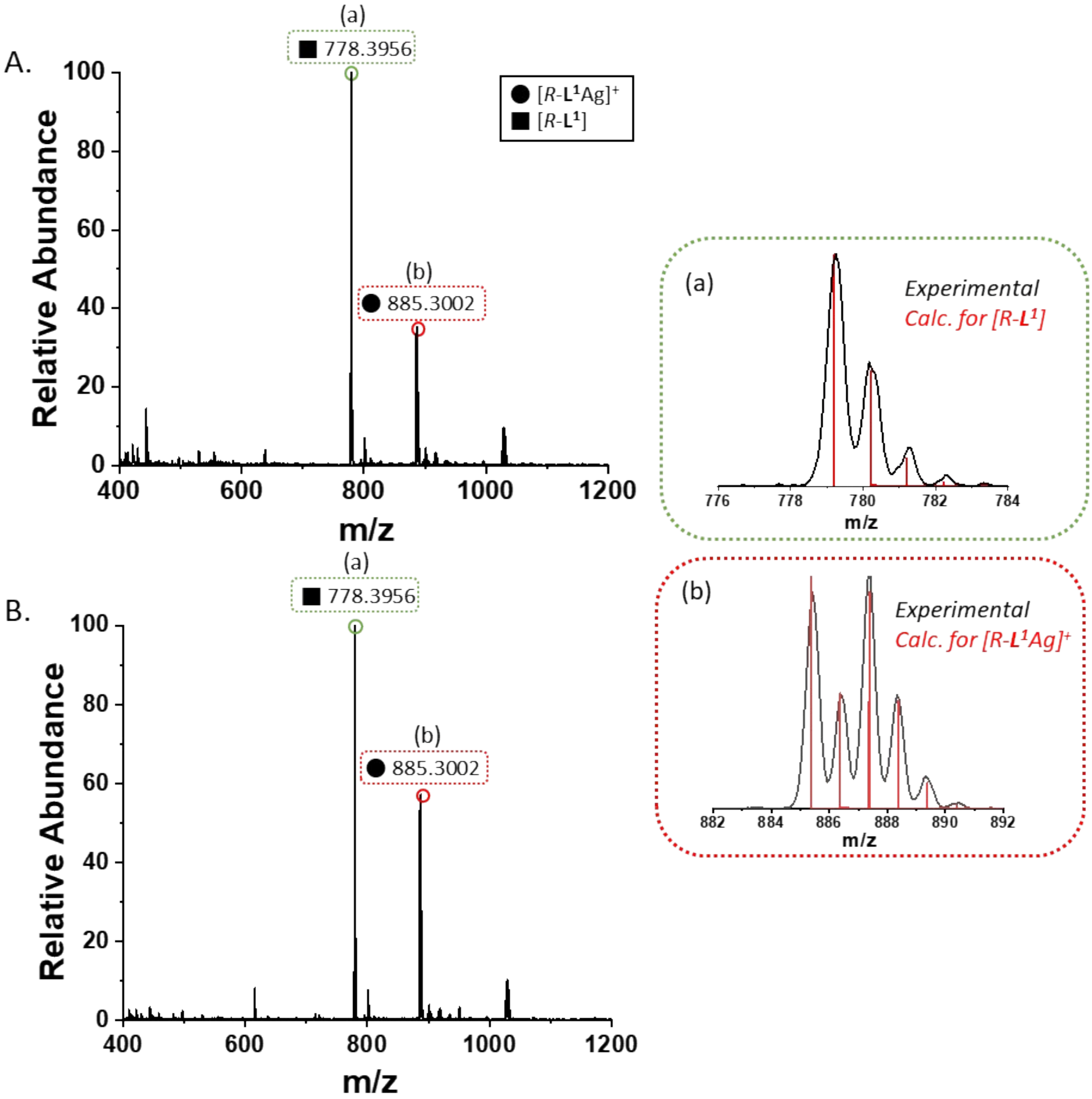

Fig. S2 HR-ESI-MS spectra of *R*-**L**^{1} (6.4 mM) in the presence of different equiv. of $AgNO_3$: (A) 0.3 equiv. and (B) 0.4 equiv. in DMSO/H_2O (1:1 v/v) after 72 h aging.

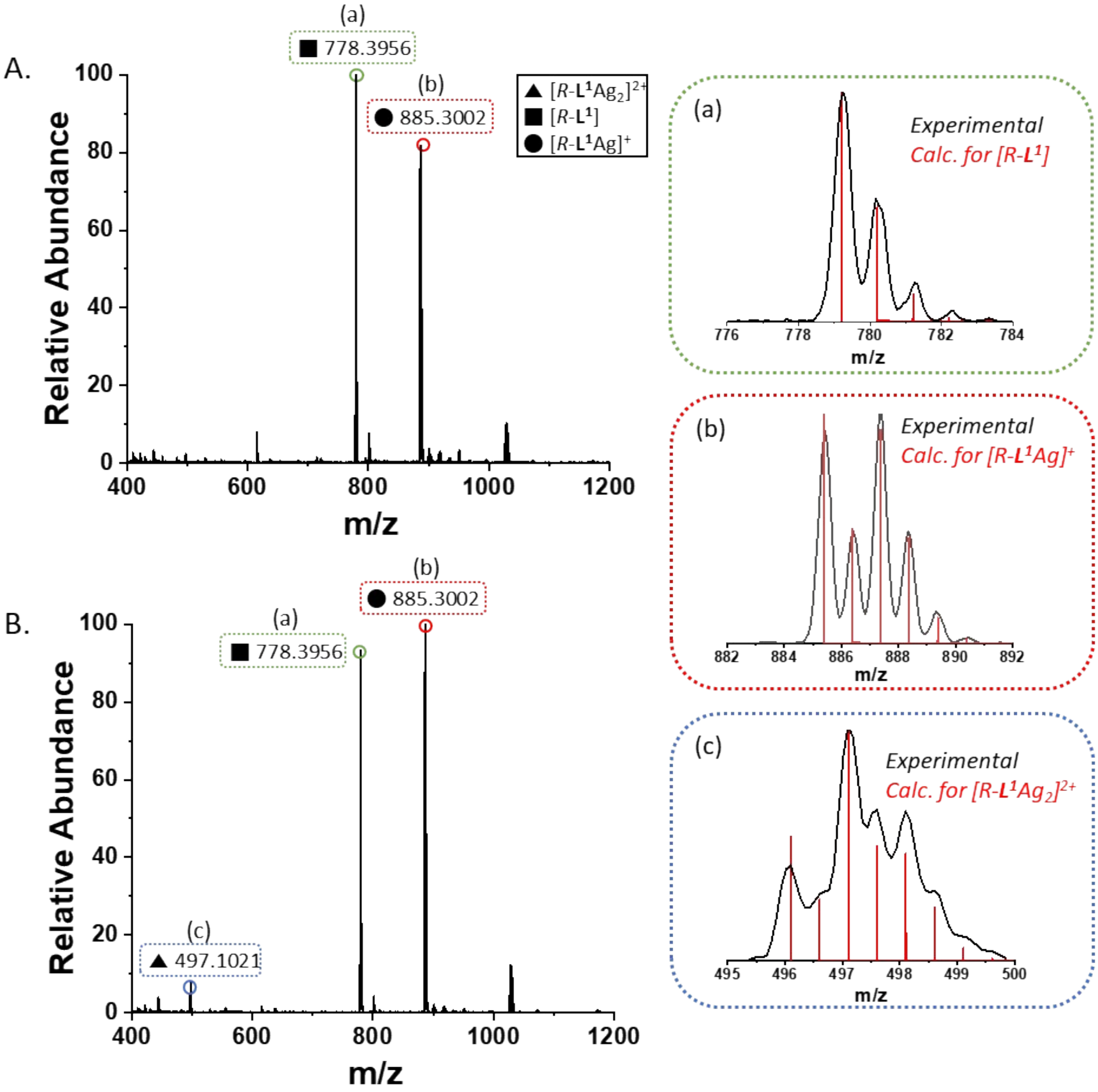

Fig. S3 HR-ESI-MS spectra of *R*-**L**^{1} (6.4 mM) in the presence of different equiv. of $AgNO_3$; (A) 0.5 equiv. and (B) 0.6 equiv. in DMSO/H_2O (1:1 v/v) after 72 h aging.

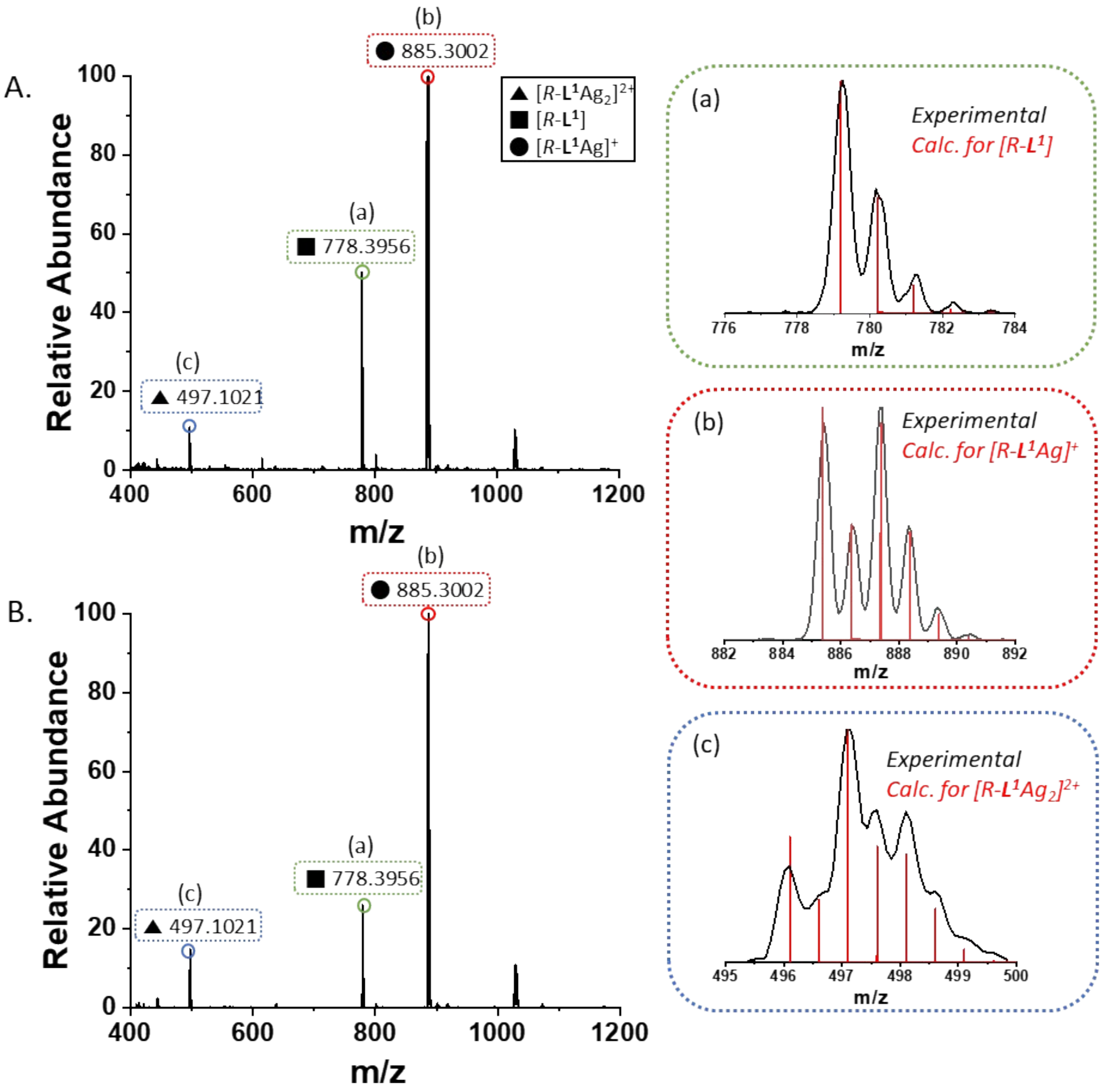

Fig. S4 HR-ESI-MS spectra of *R*-**L**^{1} (6.4 mM) in the presence of different equiv. of $AgNO_3$; (A) 0.8 equiv. and (B) 1.0 equiv. in DMSO/H_2O (1:1 v/v) after 72 h aging.

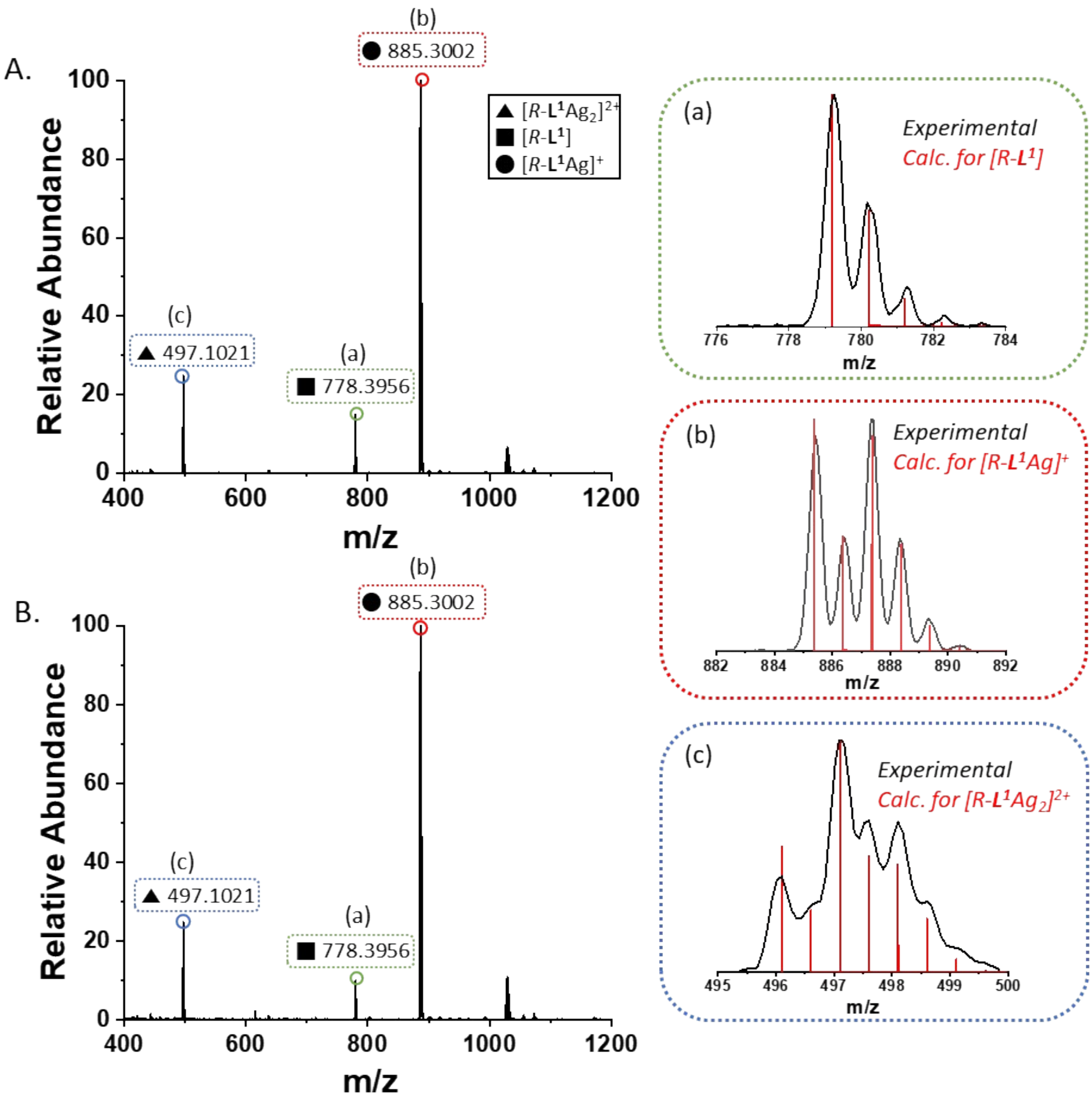

Fig. S5 HR-ESI-MS spectra of *R*-**L**^{1} (6.4 mM) in the presence of different equiv. of $AgNO_3$; (A) 1.2 equiv. and (B) 1.4 equiv. in DMSO/H_2O (1:1 v/v) after 72 h aging.

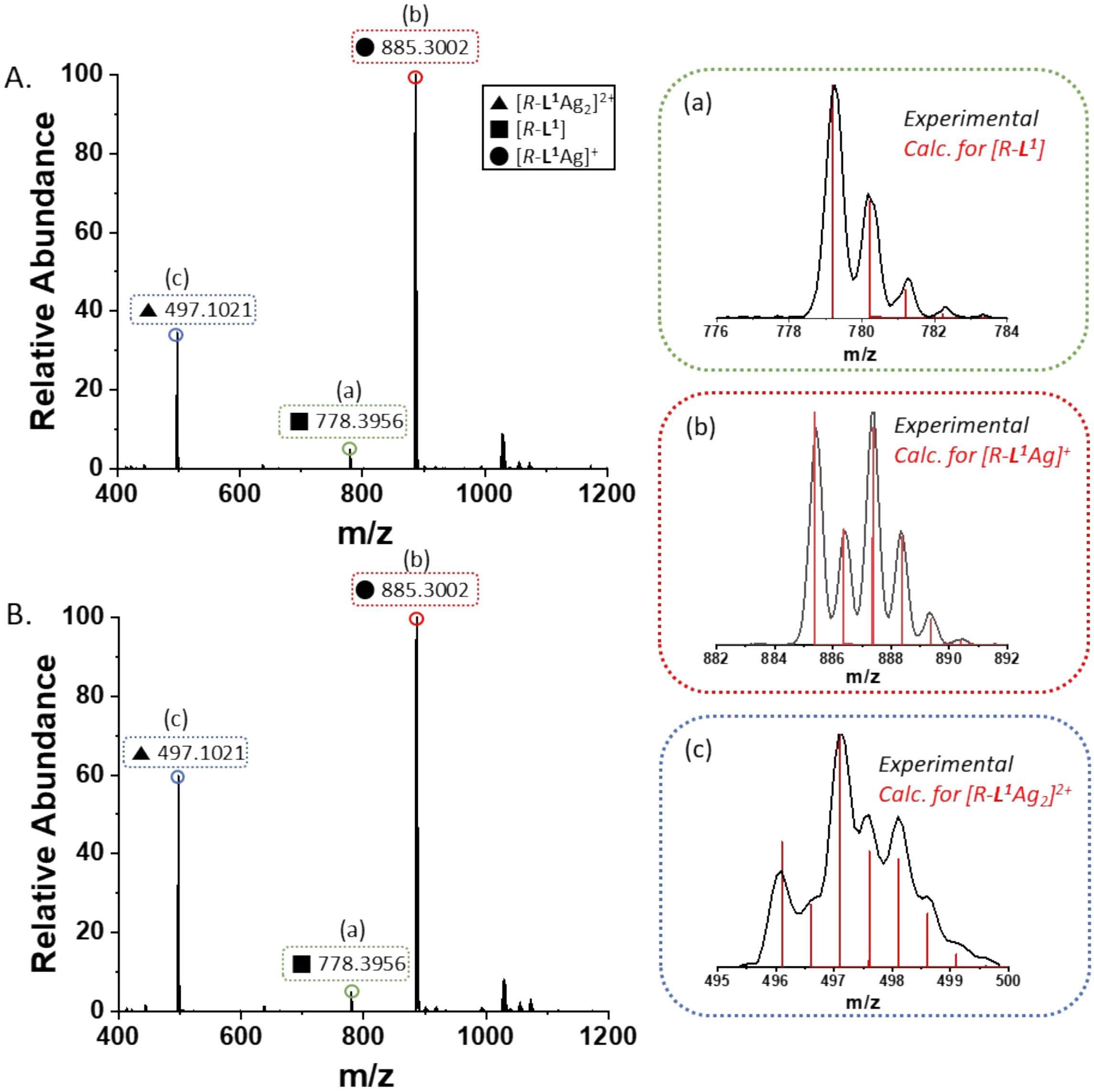

Fig. S6 HR-ESI-MS spectra of *R*-**L**^{1} (6.4 mM) in the presence of different equiv. of $AgNO_3$; (A) 1.6 equiv., and (B) 1.8 equiv. in DMSO/H_2O (1:1 v/v) after 72 h aging.

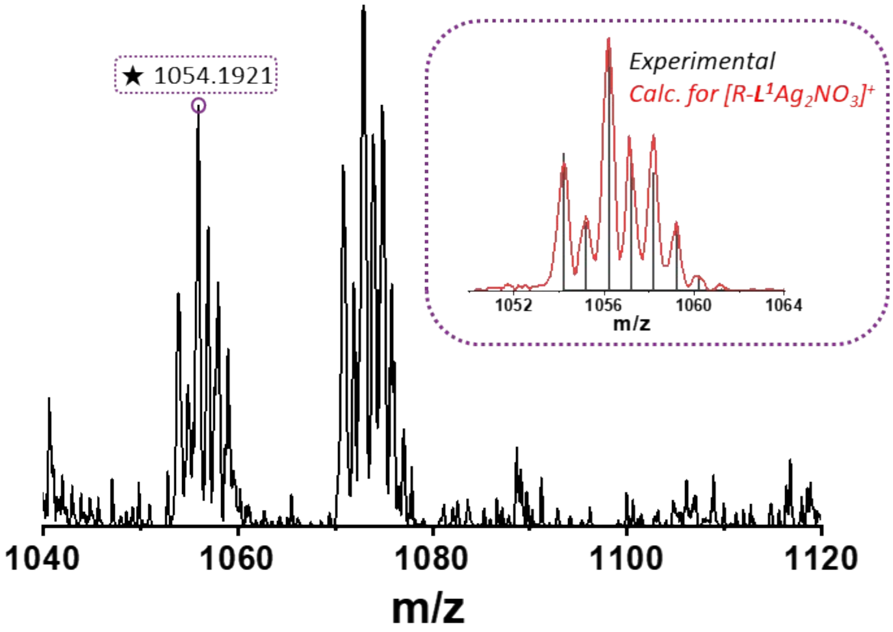

Fig. S7 HR-ESI-MS spectrum of [R-$\mathbf{L}^1$Ag$_2$NO$_3$]$^+$.

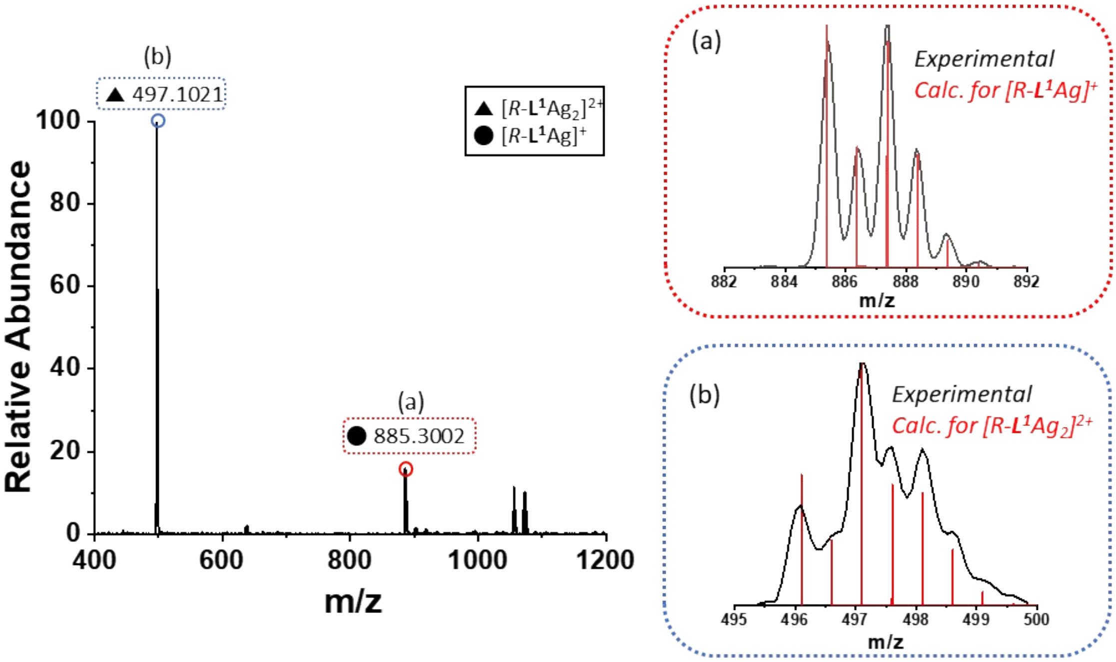

Fig. S8 HR-ESI-MS spectrum of R-$\mathbf{L}^1$ (6.4 mM) in the presence of AgNO$_3$ (2.0 equiv.) in DMSO/H$_2$O (1:1 v/v) after 72 h aging.

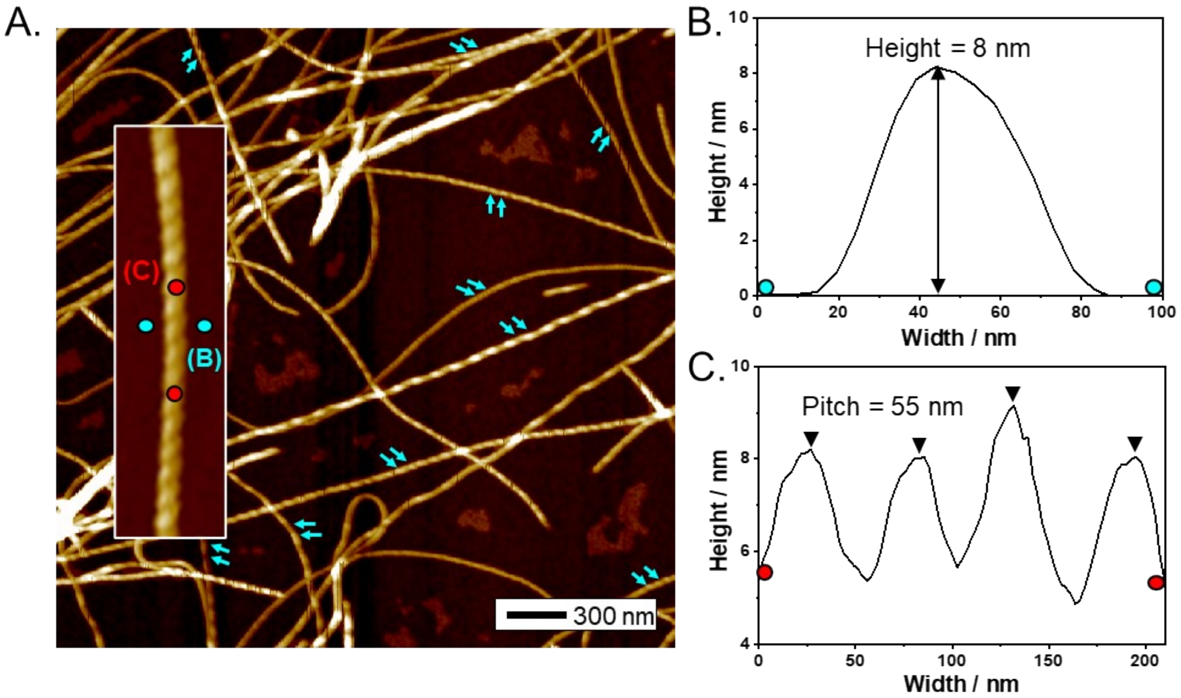

Fig. S9 (A) AFM image of R-$\mathbf{L}^1$ (6.4 mM) without $AgNO_3$ in DMSO/H_2O (1:1 v/v) after 72 h aging. Cross-sectional analysis (B) blue dots (for height) and (C) red dots (for pitch) in the image.

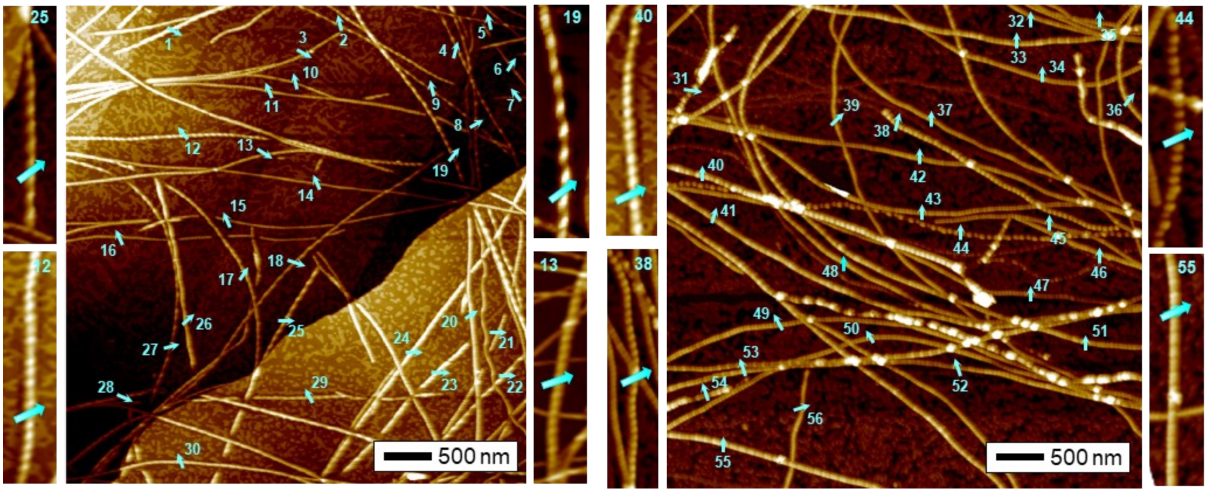

Fig. S10 AFM images of R-$\mathbf{L}^1$ (6.4 mM) in DMSO/H_2O (1:1 v/v) after 72 h aging. No shown all AFM images.

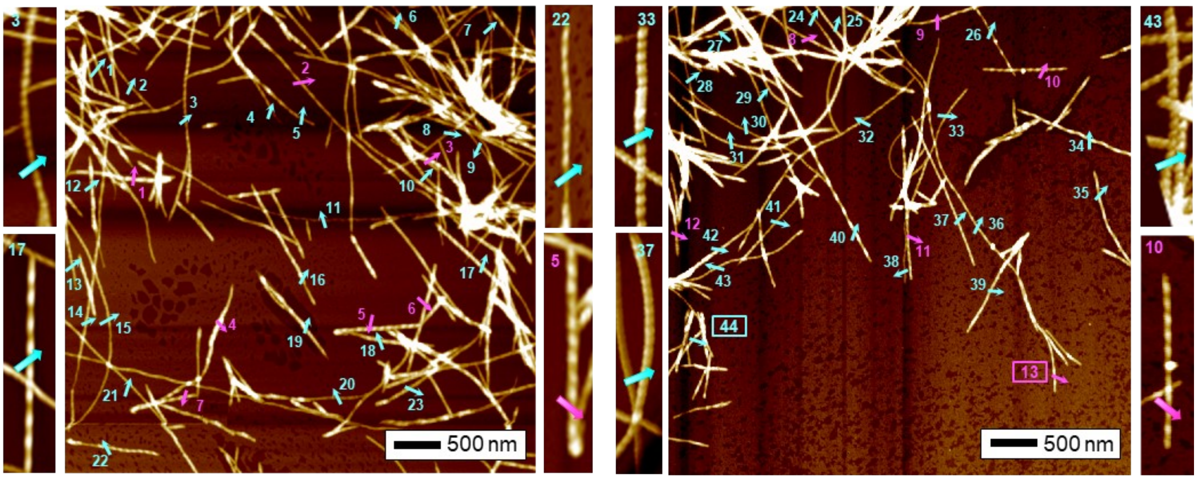

Fig. S11 AFM images of *R*-$\mathbf{L}^1$ (6.4 mM) with 0.2 equiv. of $AgNO_3$ in DMSO/H_2O (1:1 v/v) after 72 h aging. The blue arrows indicate right-handed helical fiber. The pink arrows indicate left-handed helical fiber. No shown all AFM images.

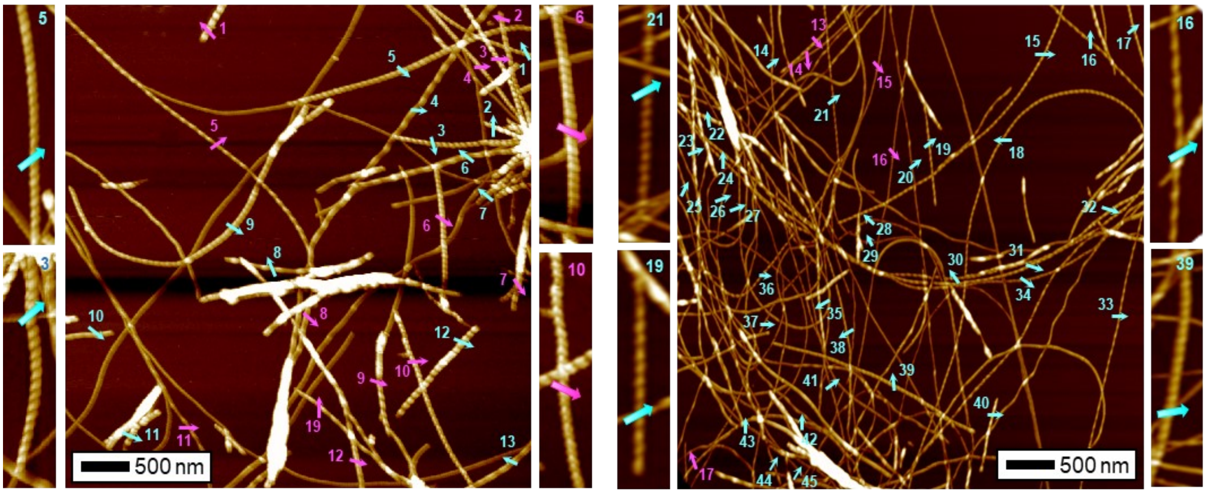

Fig. S12 AFM images of *R*-$\mathbf{L}^1$ (6.4 mM) with 0.4 equiv. of $AgNO_3$ in DMSO/H_2O (1:1 v/v) after 72 h aging. No Shown all AFM images. The blue arrows indicate right-handed helical fiber. The pink arrows indicate left-handed helical fiber.

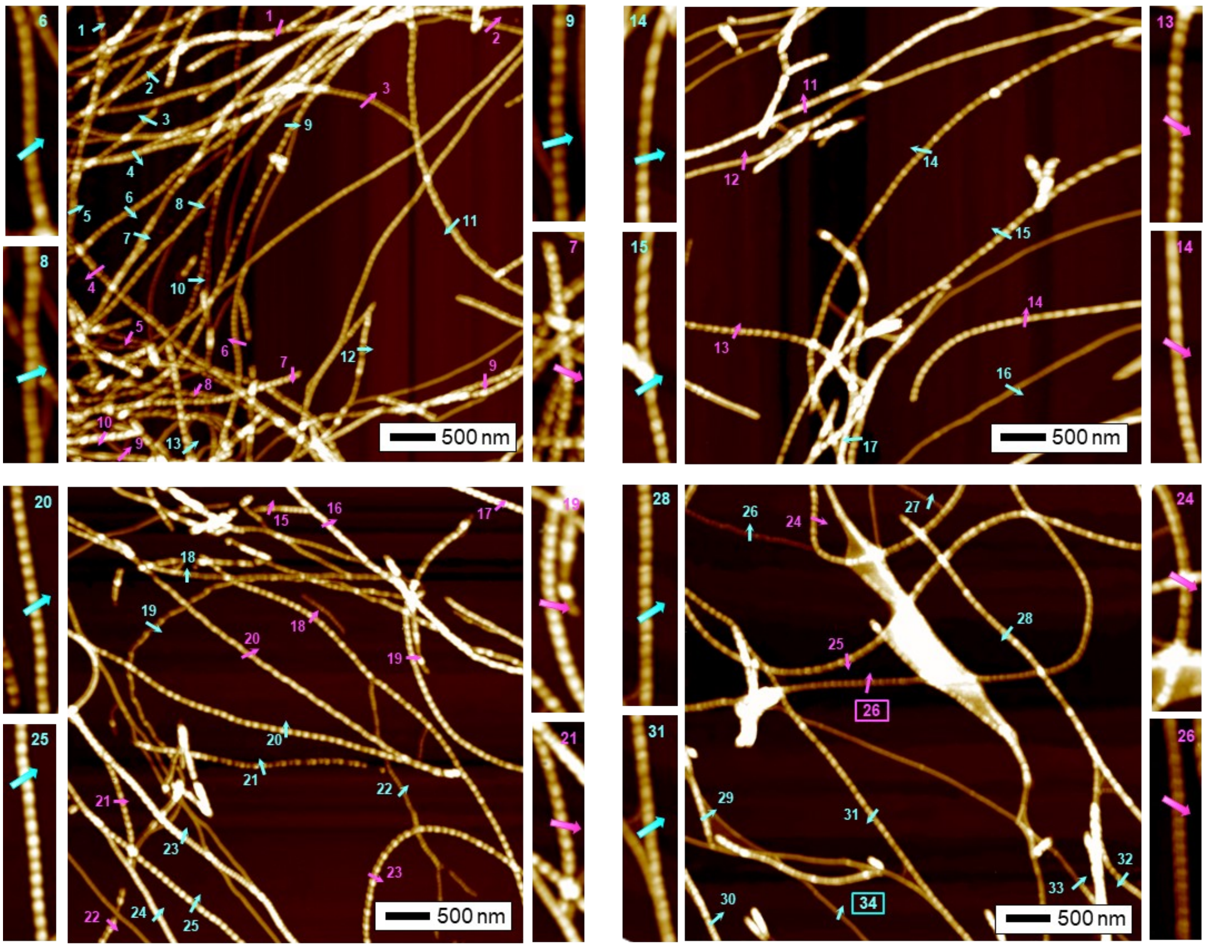

Fig. S13 AFM images of *R*-$\mathbf{L}^1$ (6.4 mM) with 0.6 equiv. of $AgNO_3$ in DMSO/H_2O (1:1 v/v) after 72 h aging. No shown all AFM images. The blue arrows indicate right-handed helical fiber. The pink arrows indicate left-handed helical fiber.

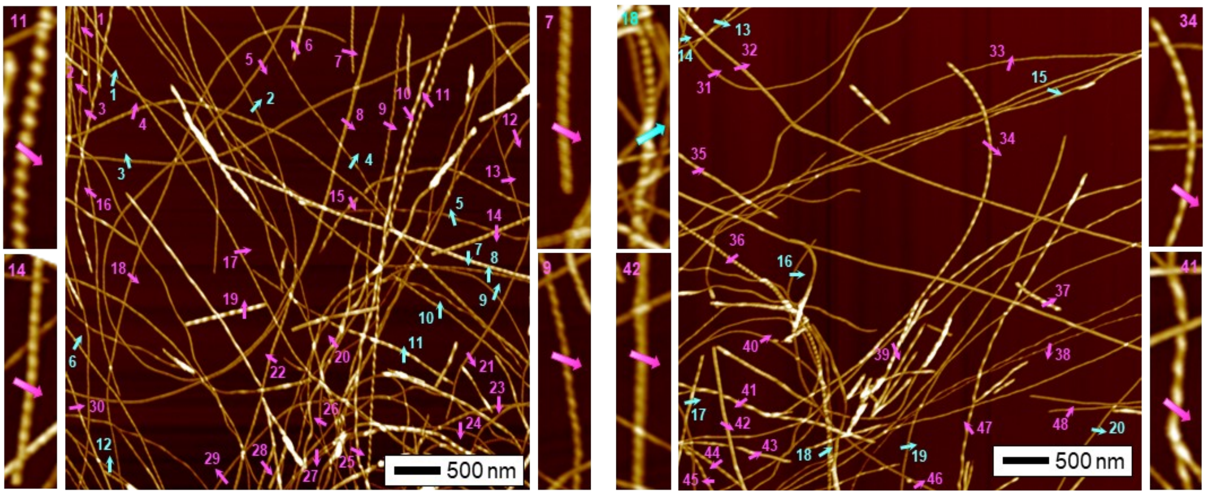

Fig. S14 AFM images of *R*-**L**^{1} (6.4 mM) with 0.8 equiv. of $AgNO_3$ in DMSO/H_2O (1:1 v/v) after 72 h aging. No shown all AFM images. The blue arrows indicate right-handed helical fiber. The pink arrows indicate left-handed helical fiber.

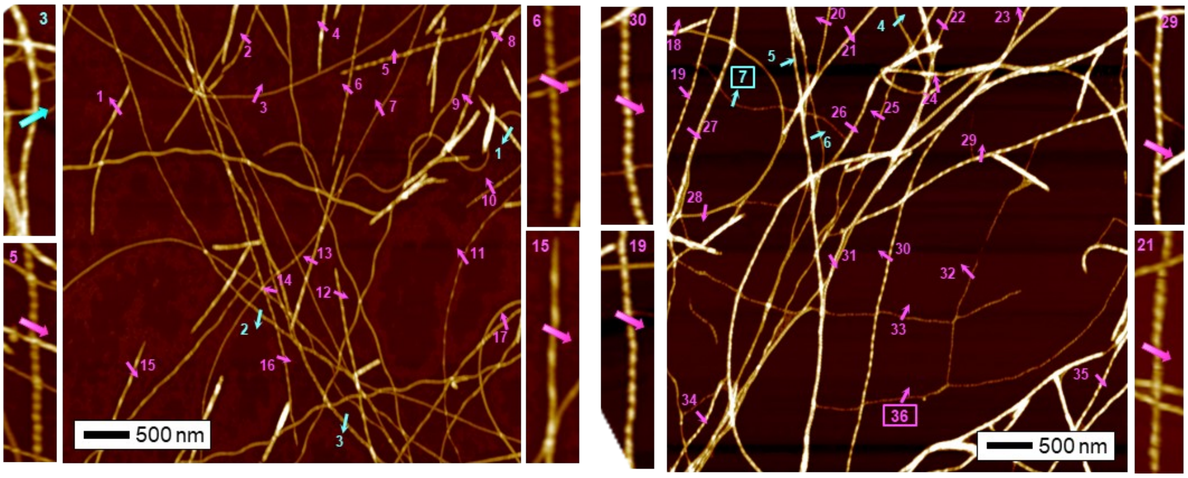

Fig. S15 AFM images of *R*-**L**^{1} (6.4 mM) with 1.0 equiv. of $AgNO_3$ in DMSO/H_2O (1:1 v/v) after 72 h aging. No shown all AFM images. The blue arrows indicate right-handed helical fiber. The pink arrows indicate left-handed helical fiber.

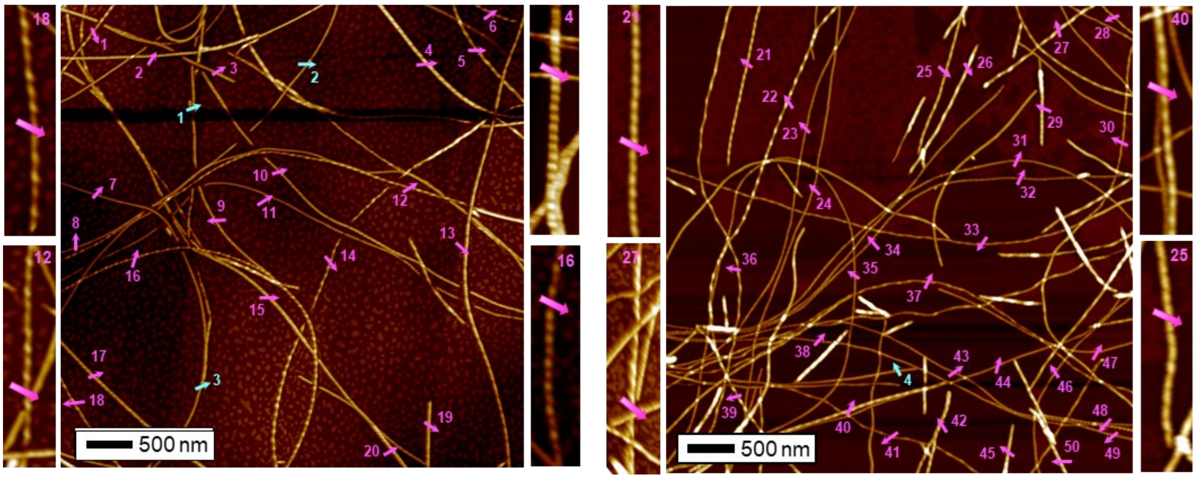

Fig. S16 AFM images of *R*-**L**^{1} (6.4 mM) with 1.2 equiv. of $AgNO_3$ in DMSO/H_2O (1:1 v/v) after 72 h aging. No shown all AFM images. The blue arrows indicate right-handed helical fiber. The pink arrows indicate left-handed helical fiber.

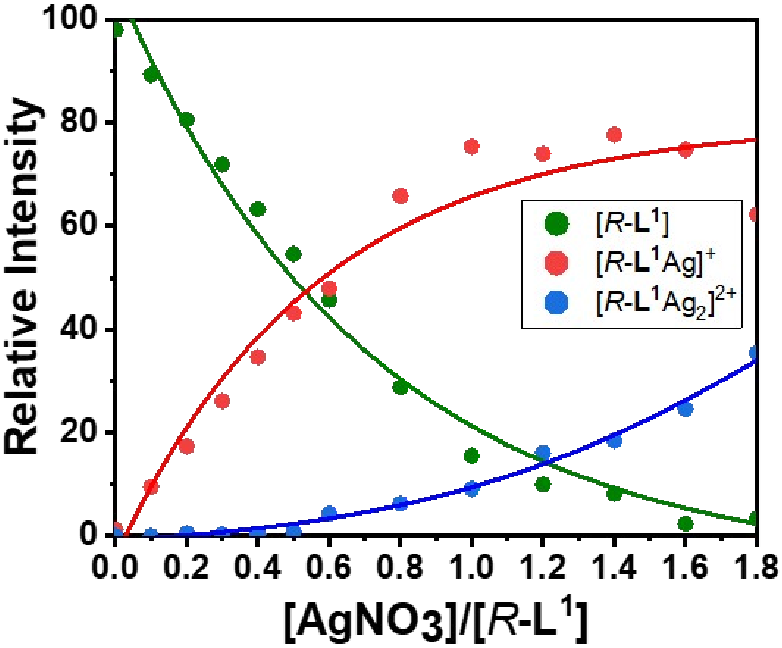

Fig. S17 Species distribution depending on $[AgNO_3]$/[*R*-**L**^{1}] ratios monitored by ESI-MS.

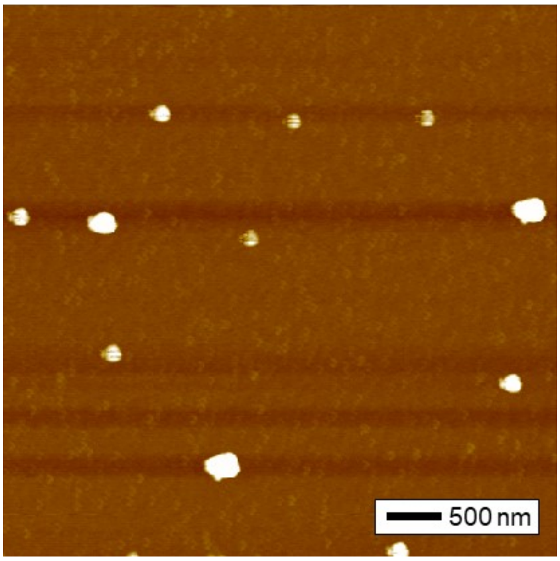

Fig. S18 AFM images of *R*-**L**^{1} (6.4 mM) with 2.0 equiv. of $AgNO_3$ in DMSO/H_2O (1:1 v/v) after 72 h aging.

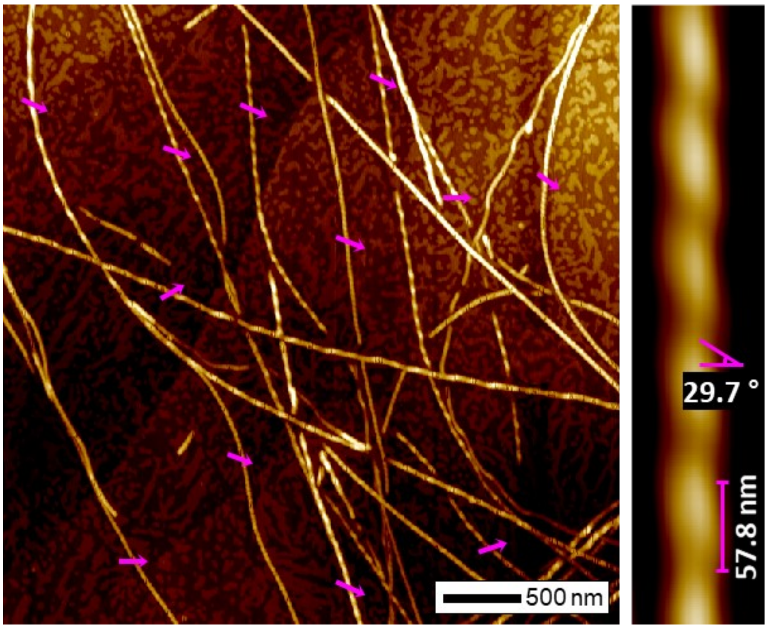

Fig. S19 AFM image of *S*-**L**^{1} (6.4 mM) without $AgNO_3$ in DMSO/H_2O (1:1 v/v) after 72 h aging.

[*Note*] Since unaggregated species are visible in the AFM background, we did not include the background in the calculation of right- and left-handed fibers.

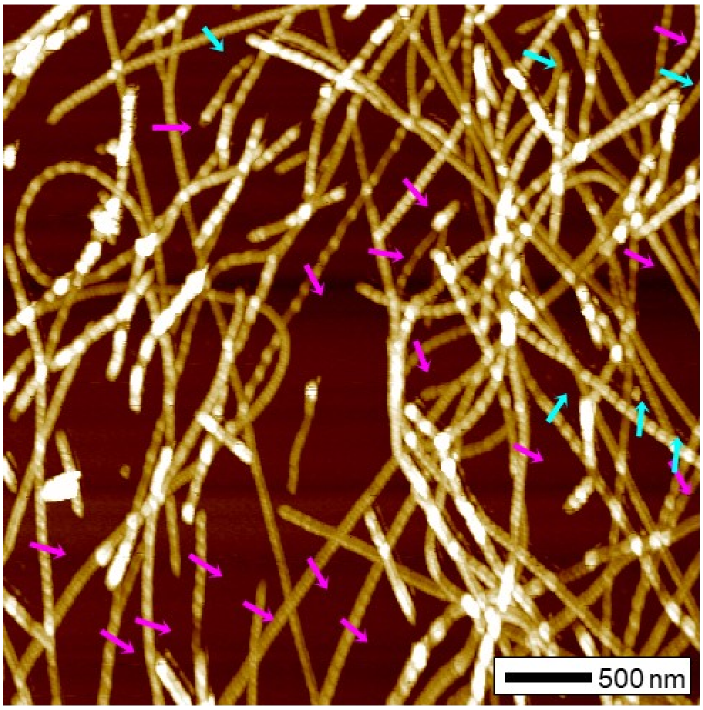

Fig. S20 AFM image of *S*-**L**^{1} (6.4 mM) with 0.2 equiv. of $AgNO_3$ in DMSO/H_2O (1:1 v/v) after 72 h aging. The blue arrows indicate right-handed helical fiber. The pink arrows indicate left-handed helical fiber.

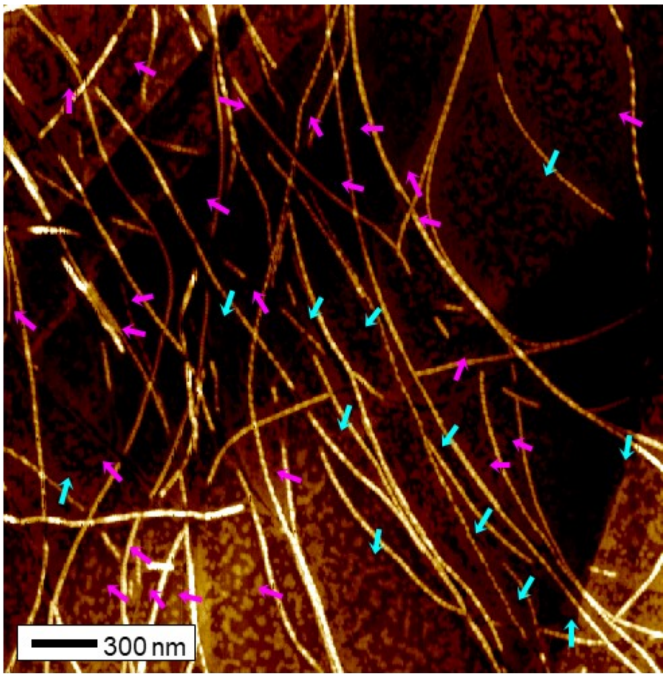

Fig. S21 AFM image of *S*-**L**^{1} (6.4 mM) with 0.4 equiv. of $AgNO_3$ in DMSO/H_2O (1:1 v/v) after 72 h aging. The blue arrows indicate right-handed helical fiber. The pink arrows indicate left-handed helical fiber.

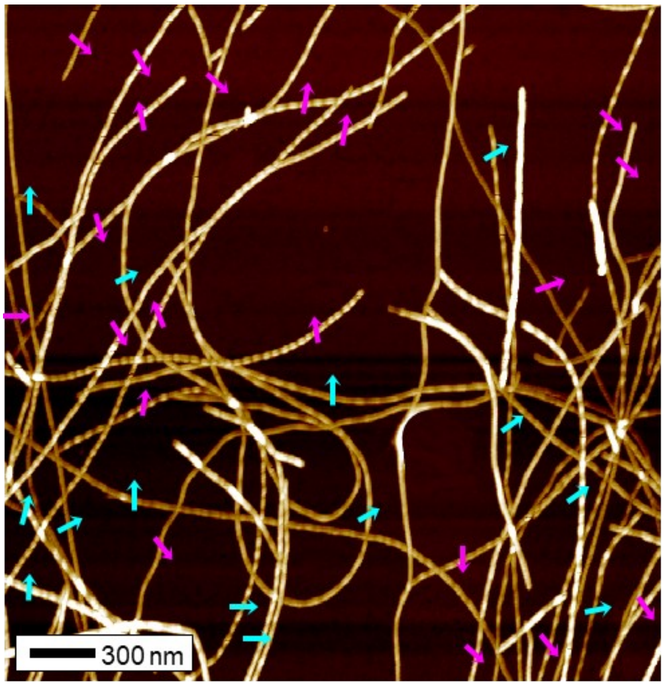

Fig. S22 AFM image of *S*-**L**^{1} (6.4 mM) with 0.6 equiv. of $AgNO_3$ in DMSO/H_2O (1:1 v/v) after 72 h aging. The blue arrows indicate right-handed helical fiber. The pink arrows indicate left-handed helical fiber.

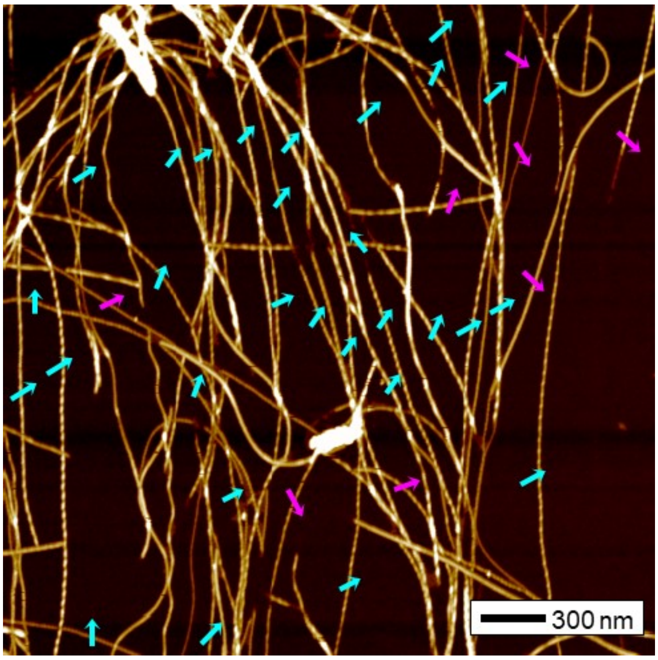

Fig. S23 AFM image of *S*-**L**^{1} (6.4 mM) with 0.8 equiv. of $AgNO_3$ in DMSO/H_2O (1:1 v/v) after 72 h aging. The blue arrows indicate right-handed helical fiber. The pink arrows indicate left-handed helical fiber.

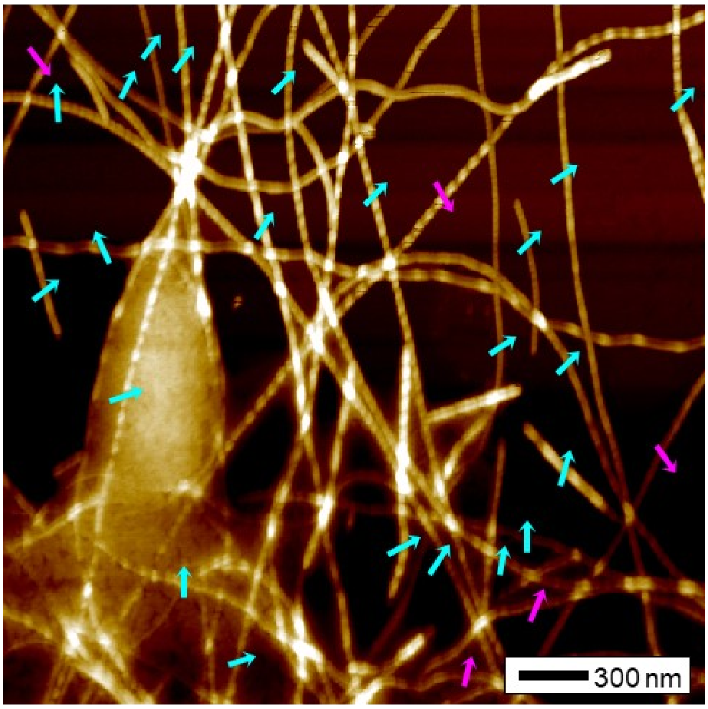

Fig. S24 AFM image of *S*-**L**^{1} (6.4 mM) with 1.0 equiv. of $AgNO_3$ in DMSO/H_2O (1:1 v/v) after 72 h aging. The blue arrows indicate right-handed helical fiber. The pink arrows indicate left-handed helical fiber.

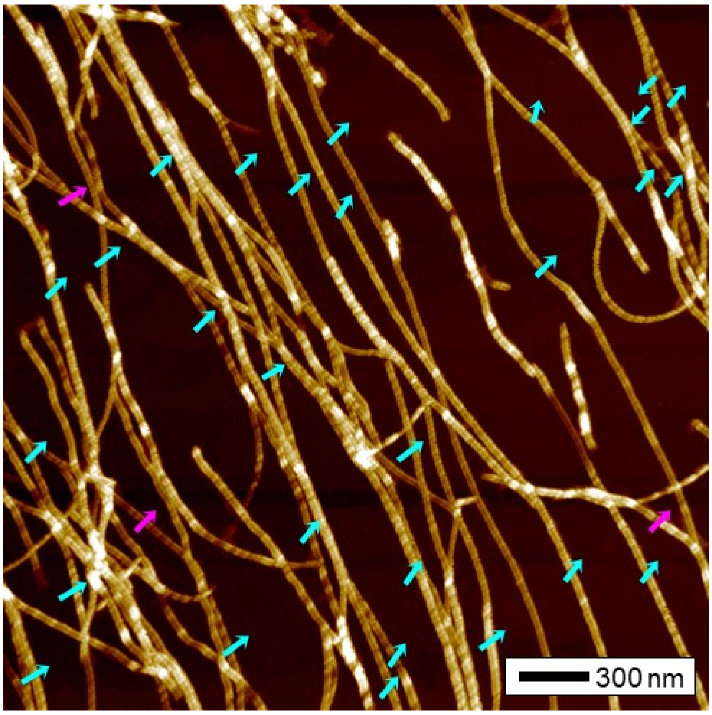

Fig. S25 AFM image of *S*-**L**^{1} (6.4 mM) with 1.2 equiv. of $AgNO_3$ in DMSO/H_2O (1:1 v/v) after 72 h aging. The blue arrows indicate right-handed helical fiber. The pink arrows indicate left-handed helical fiber.

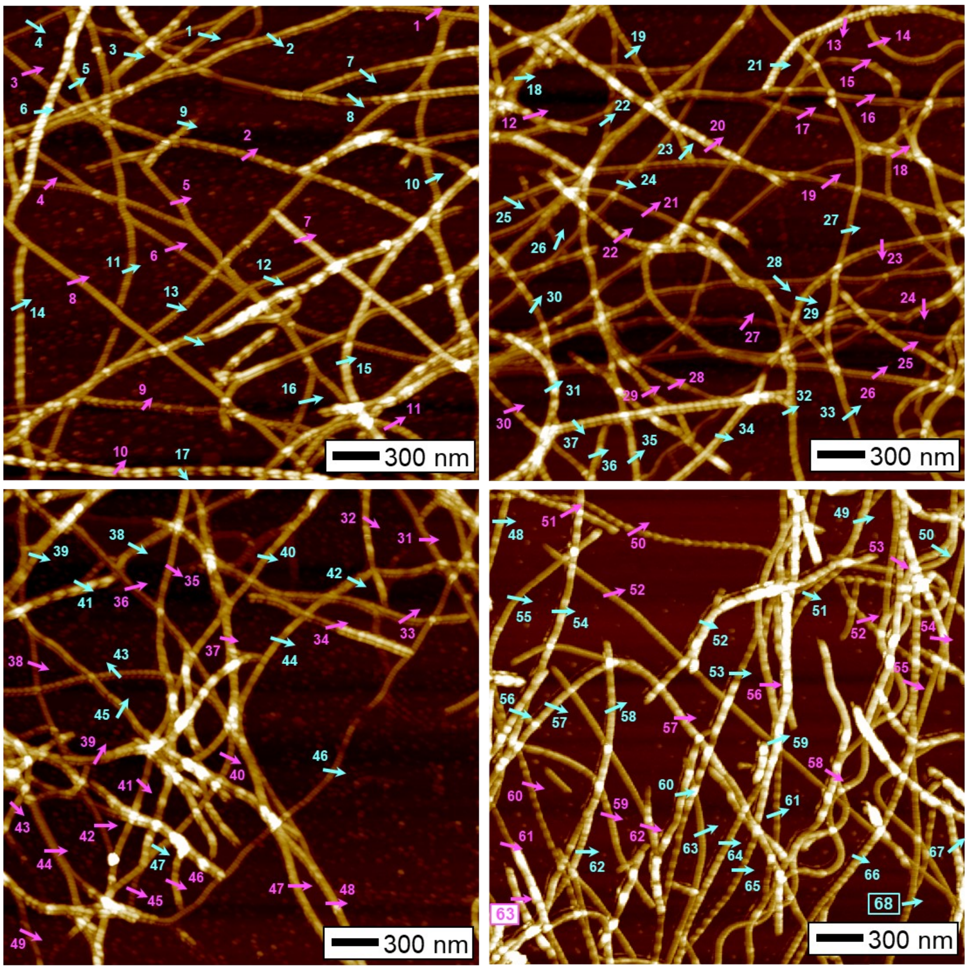

Fig. S26 AFM images of a mixure of R-**L**^{1} (6.4 mM) and S-**L**^{1} (6.4 mM) without $AgNO_3$ in DMSO/H_2O (1:1 v/v) after 72 h aging. The blue arrows indicate right-handed helical fiber. The pink arrows indicate left-handed helical fiber.

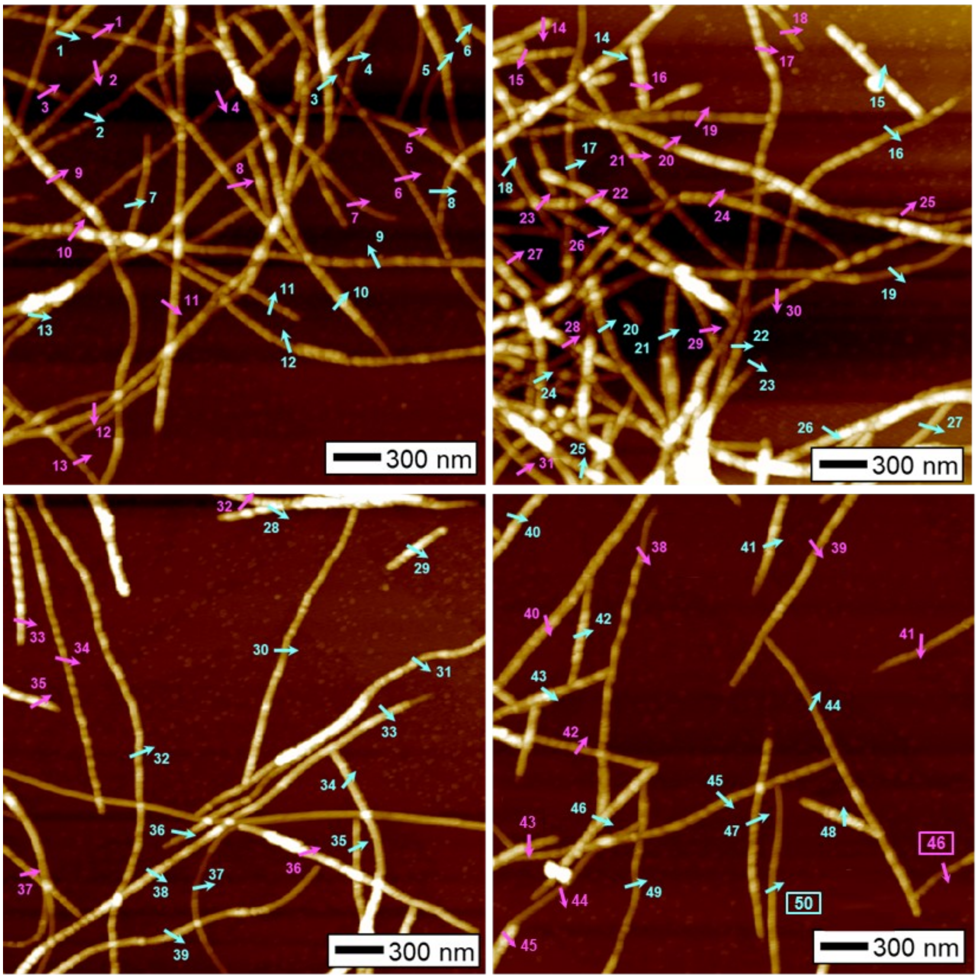

Fig. S27 AFM image of a mixure of *R*-**L**¹ (6.4 mM) and *S*-**L**¹ (6.4 mM) with 0.6 equiv. of $AgNO_3$ in DMSO/H_2O (1:1 v/v) after 72 h aging. The blue arrows indicate right-handed helical fiber. The pink arrows indicate left-handed helical fiber.

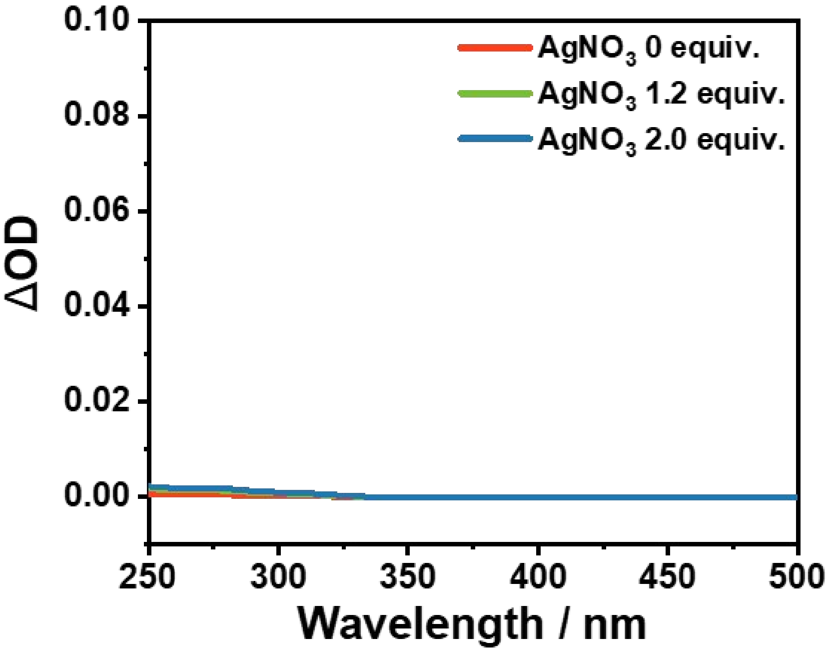

Fig. S28 LD spectra of *R*-**L**^{1} (6.4 mM) with $AgNO_3$ (0, 1.2, and 2.0 equiv.) in DMSO/H_2O (1: 1 v/v) after 72 h aging.

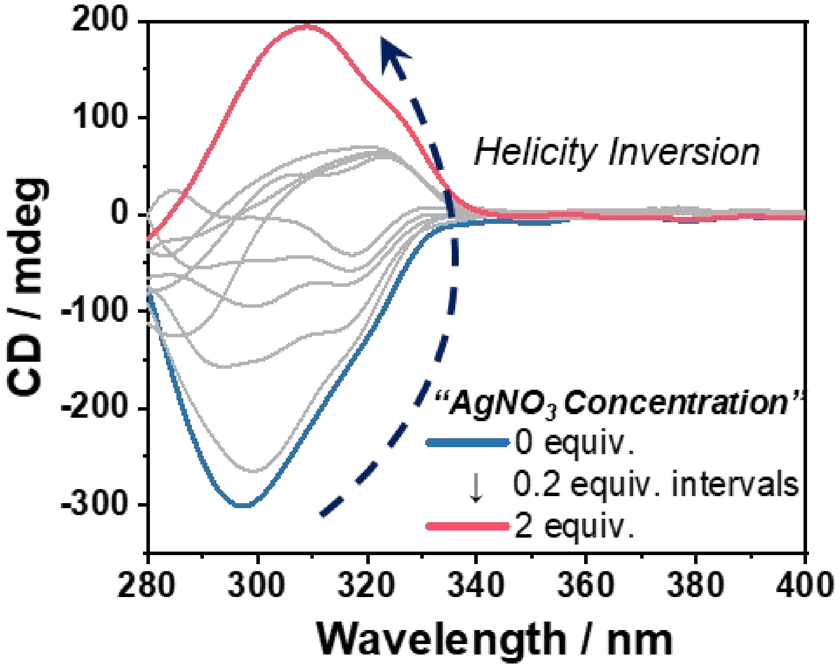

Fig. S29 CD spectra of *S*-**L**^{1} (8 mM) upon stepwise addition of $AgNO_3$ (0-2.0 equiv.) in DMSO/H_2O (1:1 v/v). The negative signal observed at ~297 nm (blue line) originates from free *S*-**L**^{1}, while the positive signal at ~307 nm (red line) originates from [*S*-**L**^{1}Ag]$^+$.

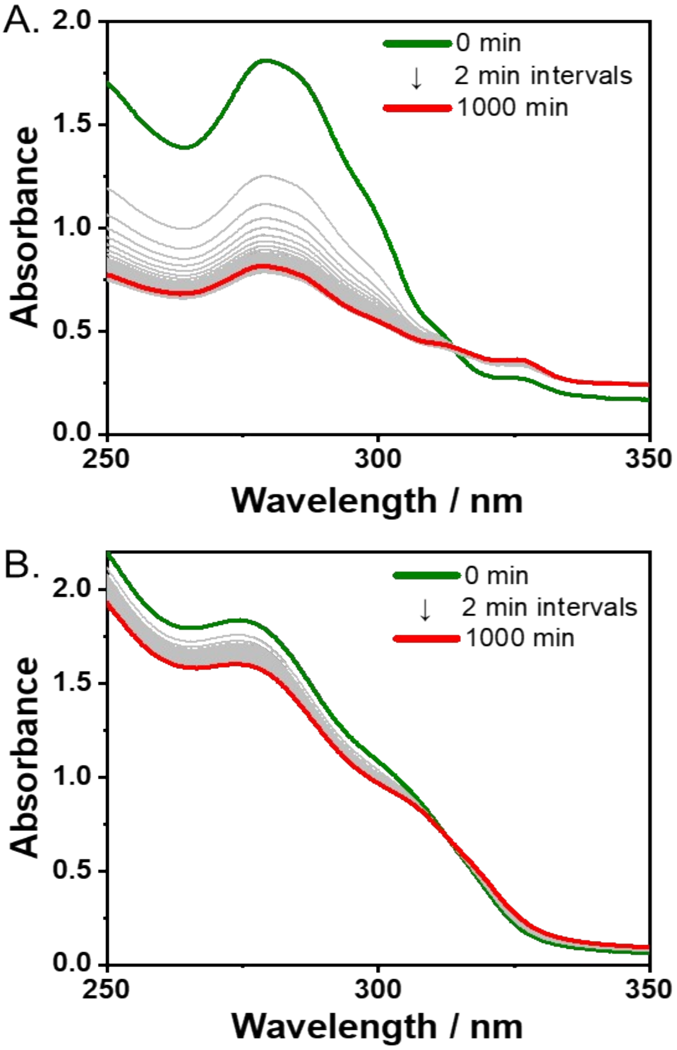

Fig. S30 Time-dependent (0-1000 min) UV-vis spectra of R-$\mathbf{L}^1$ (7.2 mM) in the presence of different equiv. of $AgNO_3$ in DMSO/H_2O (1:1 v/v) (cell path length: 0.2 mm): (a) 0 equiv. and (b) 0.4 equiv.

[*Note*] To elucidate the supramolecular polymerization process, we first prepared the sample by dissolving R-$\mathbf{L}^1$ (7.2 mM) in H_2O/DMSO (1:1 v/v). After adding the sample to the UV cell, it was heated to 90 °C (1 °C/min) to form the monomeric species in UV-vis spectroscopy. Then the sample was cooled to 20 °C (5 °C/min) in UV-vis spectroscopy. The time-dependent UV-vis spectral changes were measured at 20 °C.

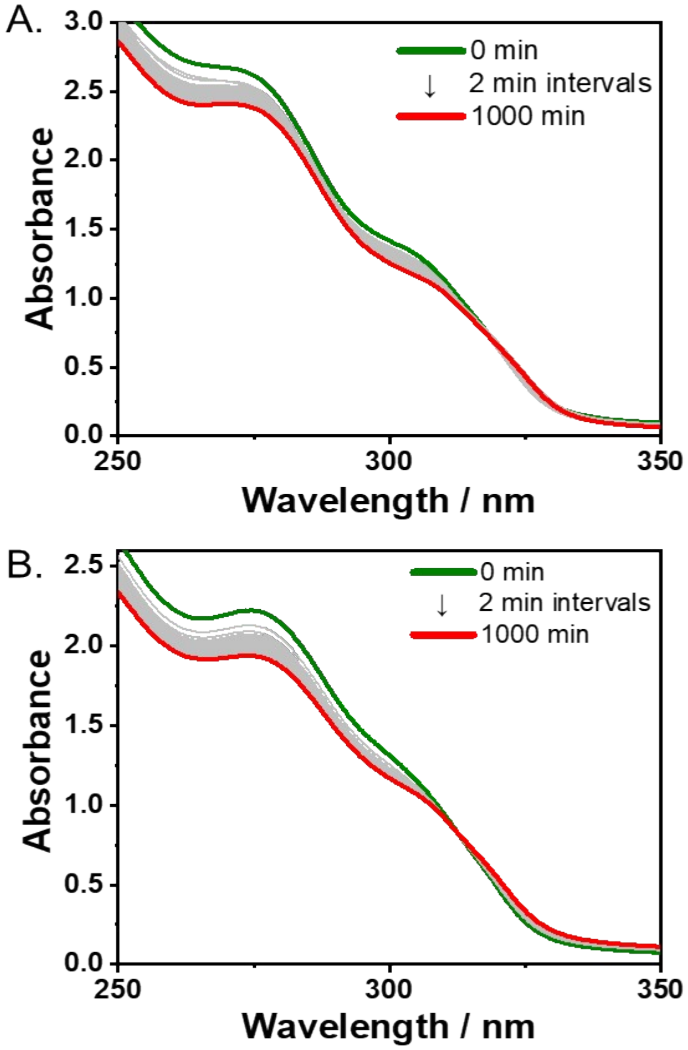

Fig. S31 Time-dependent (0-1000 min) UV-vis spectra of *R*-**L**^{1} (7.2 mM) in the presence of different equiv. of $AgNO_3$ in DMSO/H_2O (1:1 v/v) (cell path length: 0.2 mm): (a) 0.6 equiv. and (b) 0.8 equiv.

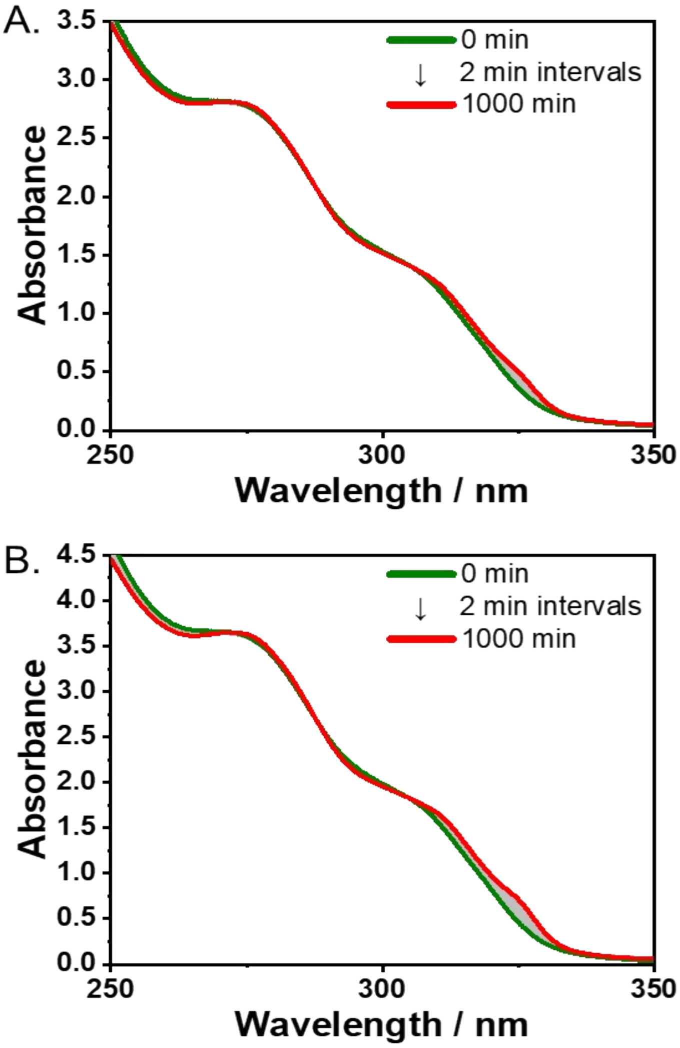

Fig. S32 Time-dependent (0-1000 nm) UV-vis spectra of *R*-$\mathbf{L}^1$ (7.2 mM) in the presence of different equiv. of $AgNO_3$ in DMSO/H_2O (1:1 v/v) (cell path length: 0.2 mm): (a) 1.2 equiv. and (b) 1.4 equiv.

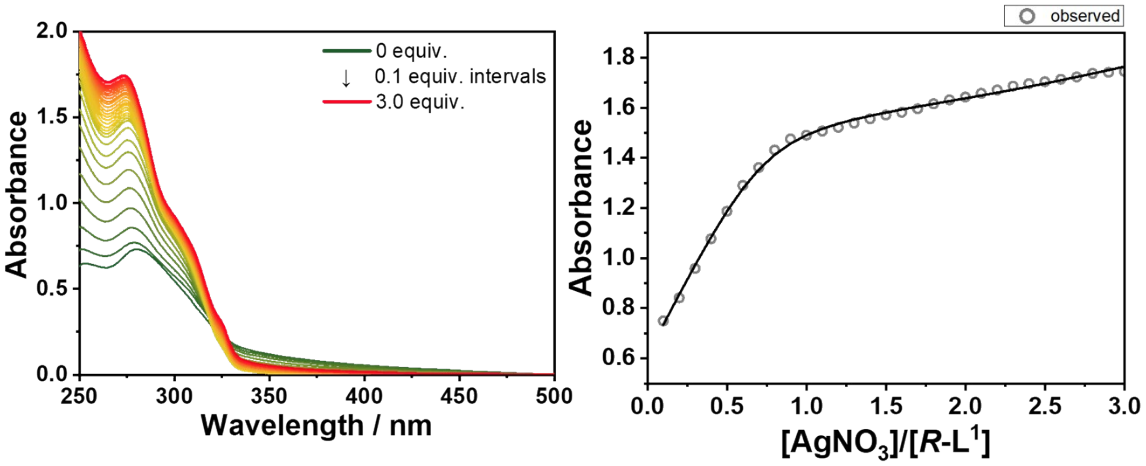

Fig. S33 Fitting of UV−vis titration data to determine the association constant for the formation of [R-$\mathbf{L}^1$Ag]$^+$ and [R-$\mathbf{L}^1$($AgNO_3$)$_2$] with HyperSpec softwareS1 by employing the 1:1 and 2:1 (Metal : L) binding model[5-7]: (a) UV-vis titration of R-$\mathbf{L}^1$ (0.05 mM) with Ag^+ (0-3.0 equiv.) in DMSO : H_2O (1:1 v/v) and (b) HyperSpec output (circle: experimental points, solid line: theoretical fit).

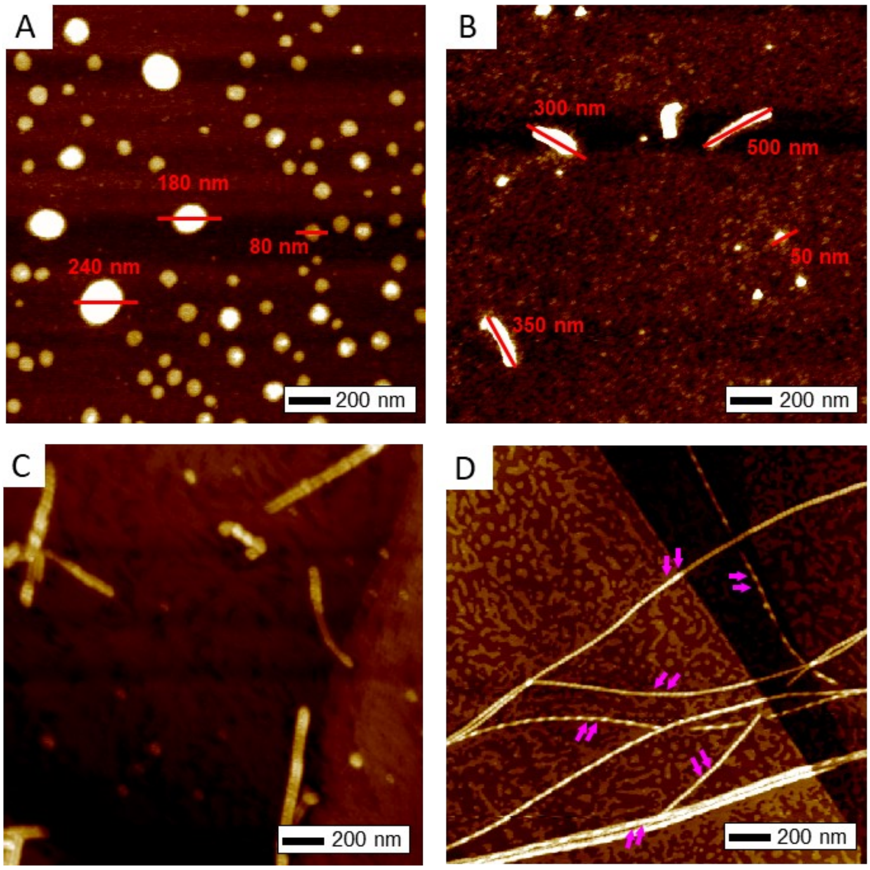

Fig. S34 Time-dependent AFM images of R-$\mathbf{L}^1$ (6.4 mM) in the presence of 1.2 equiv. of $AgNO_3$ in DMSO/H_2O (1:1 v/v). Aging times: (A) 1 h, (B) 3 h, (C) 1 day, and (D) 3 days.

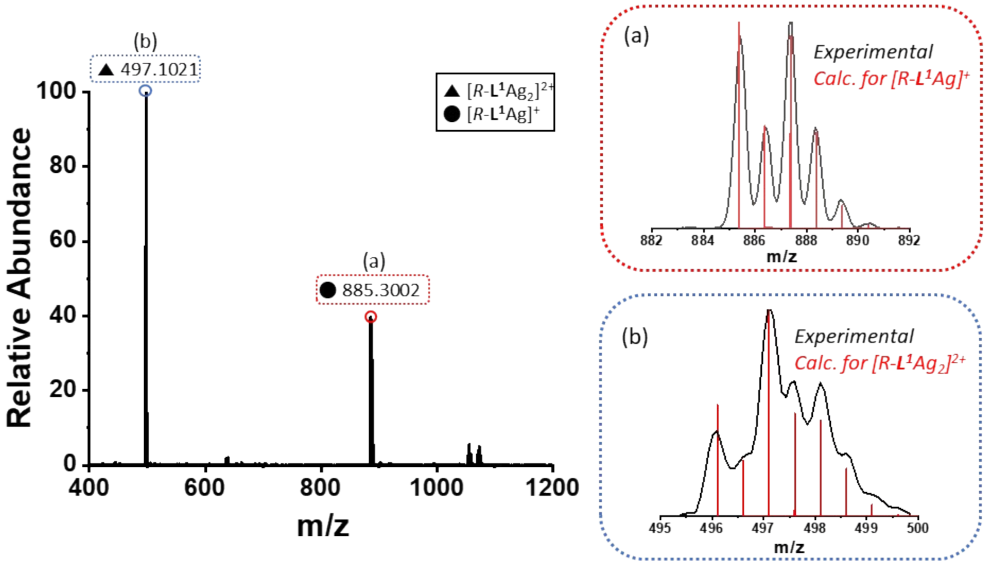

Fig. S35 ESI-MS spectrum of *R*-**L**^{1} (6.4 mM) with 1.2 equiv. of $AgNO_3$ in DMSO/H_2O (1:1 v/v) after 1 h aging.

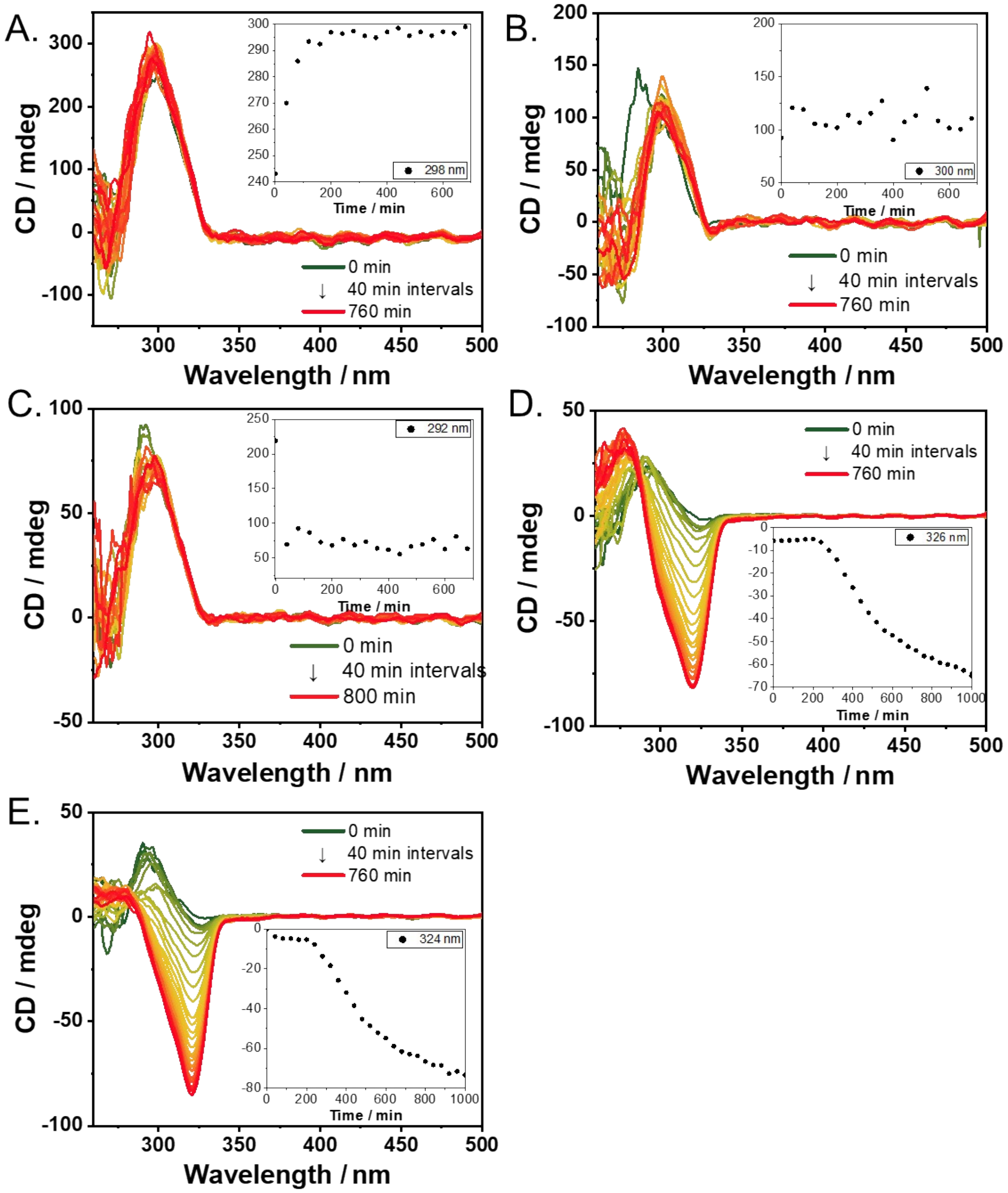

Fig. S36 Time-dependent (0-760 min) CD spectral changes of *R*-$\mathbf{L}^1$ (8 mM) in the presence of $AgNO_3$ (0-1.4 equiv.) in DMSO/H_2O (1:1 v/v) at 20 ºC (cell path length: 0.1 mm): (A) 0 equiv., (B) 0.4 equiv., (C) 0.8 equiv., (D) 1.2 equiv., and (E) 1.4 equiv.

[*Note*] To elucidate the supramolecular polymerization process, we first prepared the sample by dissolving *R*-$\mathbf{L}^1$ (7.7 mM) in H_2O/DMSO (1:1 v/v). After adding the sample to the CD cell, it was heated to 90 °C (1 °C/min) to form the monomeric species in circular dichroism (CD) spectroscopy. Then the sample was cooled to 20 °C (5 °C/min) in CD spectroscopy. The time-dependent CD spectral changes were measured at 20 °C.

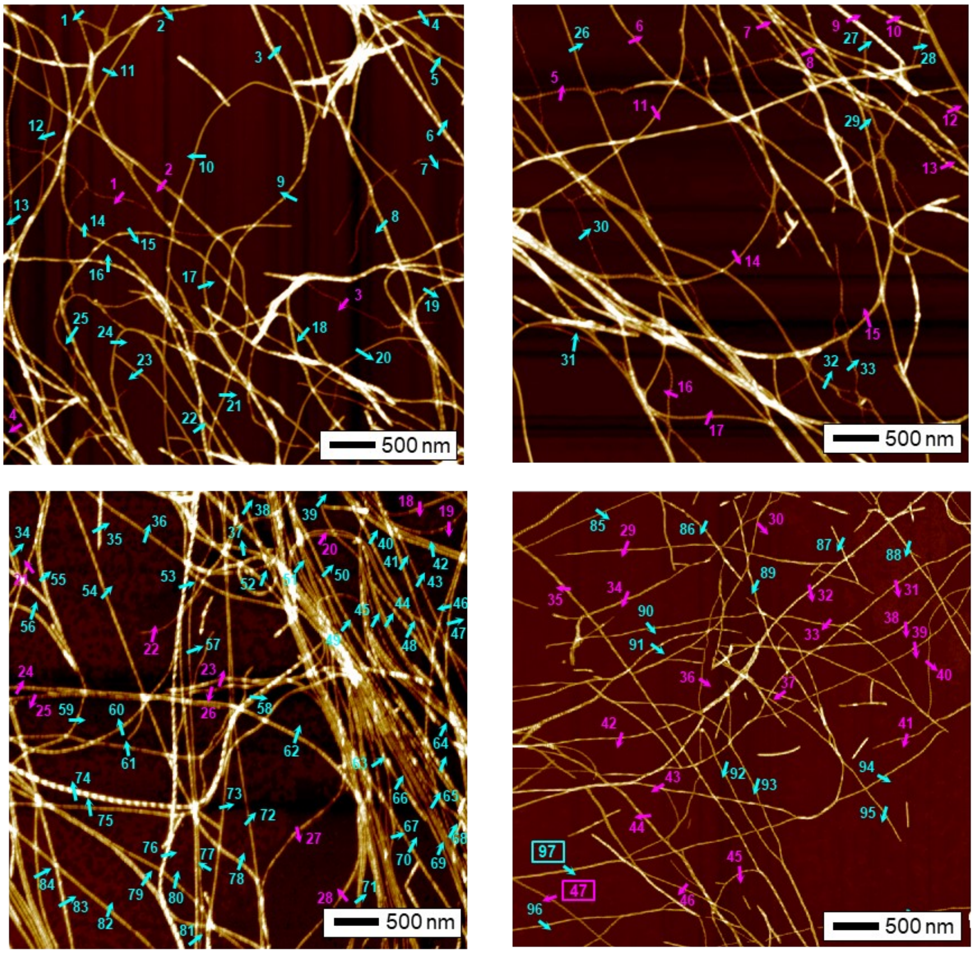

Fig. S37 AFM images of a mixed sample of aggregate I (7.2 mM, 50 μL) and aggregate III (7.2 mM, 21.5 μL) (Ag^+ : *R*-$\mathbf{L}^1$ molar ratio = 0.6) after 72 h aging. The blue arrows indicate right-handed helical fiber. The pink arrows indicate left-handed helical fiber.

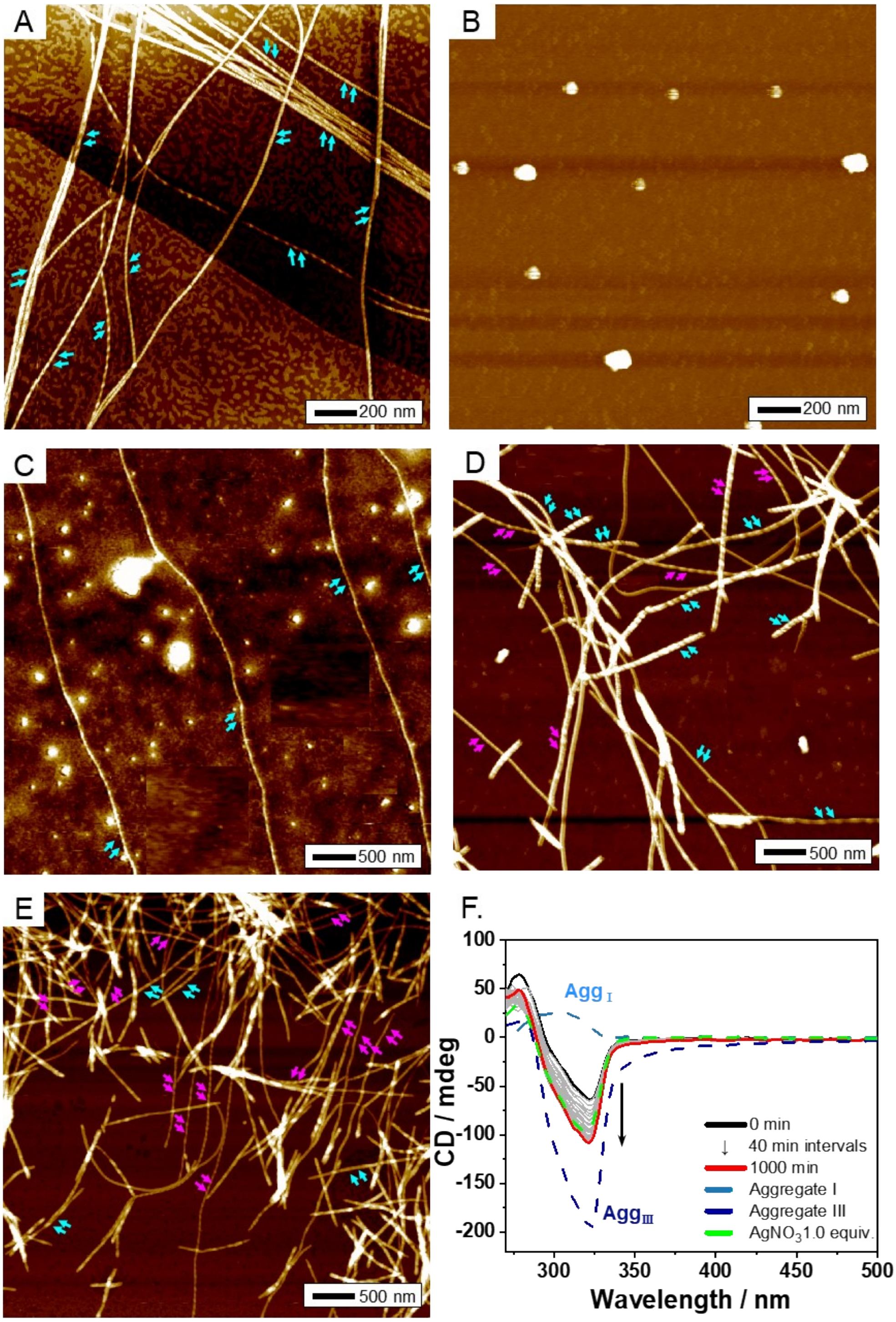

Fig. S38 AFM images of (A) aggregate I and (B) aggregate III. AFM image of a mixed sample of aggregate I (7.2 mM, 50 µL) and aggregate III (7.2 mM, 50 µL) after aging for (C) 10 min, (D) 1 h, and (E) 1 day. The molar ratio of Ag$^+$ to *R*-**L**^{1} in the mixed sample is 1.0 equiv. (F) Time-dependent CD spectra of the mixed sample of aggregate I (7.2 mM, 50 µL) and aggregate III (7.2 mM, 50 µL) in DMSO/H_2O (1:1 v/v). The blue arrows indicate right-handed helical fiber. The pink arrows indicate left-handed helical fiber.

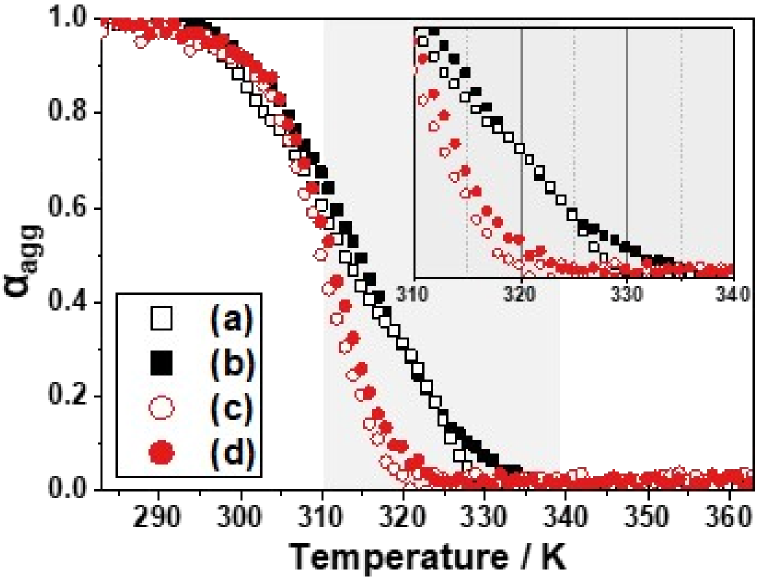

Fig. S39 Plot of CD spectral changes (at 323.5 nm) of *R*-**L**^{1} vs temperature in the presence of different equiv. of $AgNO_3$: (a) 0.6 equiv. of $AgNO_3$ and (c) 1.2 equiv. of $AgNO_3$. (b) Aggregate I (7.2 mM, 50 µL) + aggregate III (7.2 mM, 21.5 µL), consisting 0.6 equiv. of $AgNO_3$. (d) Aggregate I (7.2 mM, 50 µL) + aggregate III (7.2 mM, 75 µL), consisting 1.2 equiv. of $AgNO_3$.

[*Note*] Temperature-dependent CD spectral changes were observed by heating with 1 °C/min.

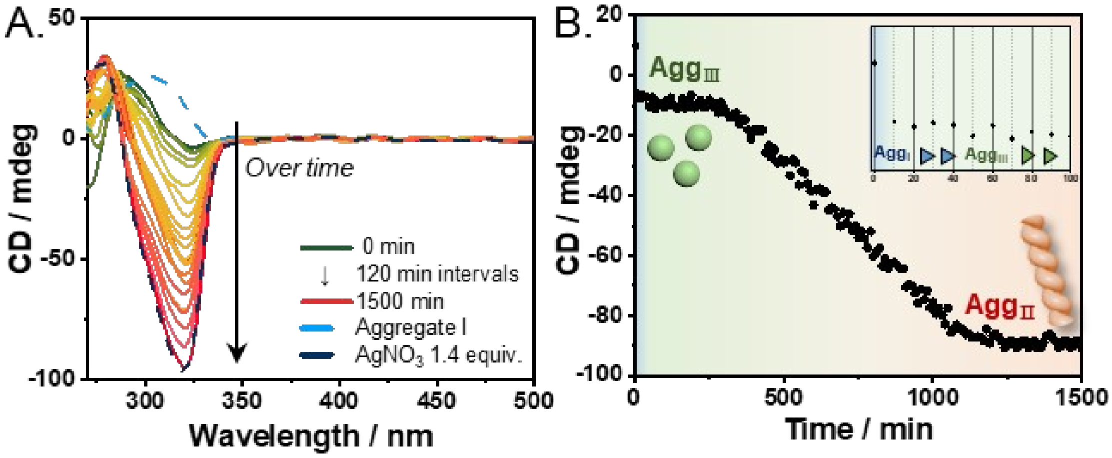

Fig. S40 (A) Time-dependent CD spectra of aggregate I upon addition of $AgNO_3$ (1.2 equiv.) in DMSO/H_2O (1:1 v/v). (B) Plot of CD spectral changes (at 323.5 nm) of aggregate I upon addition of $AgNO_3$ (1.2 equiv.) vs time.

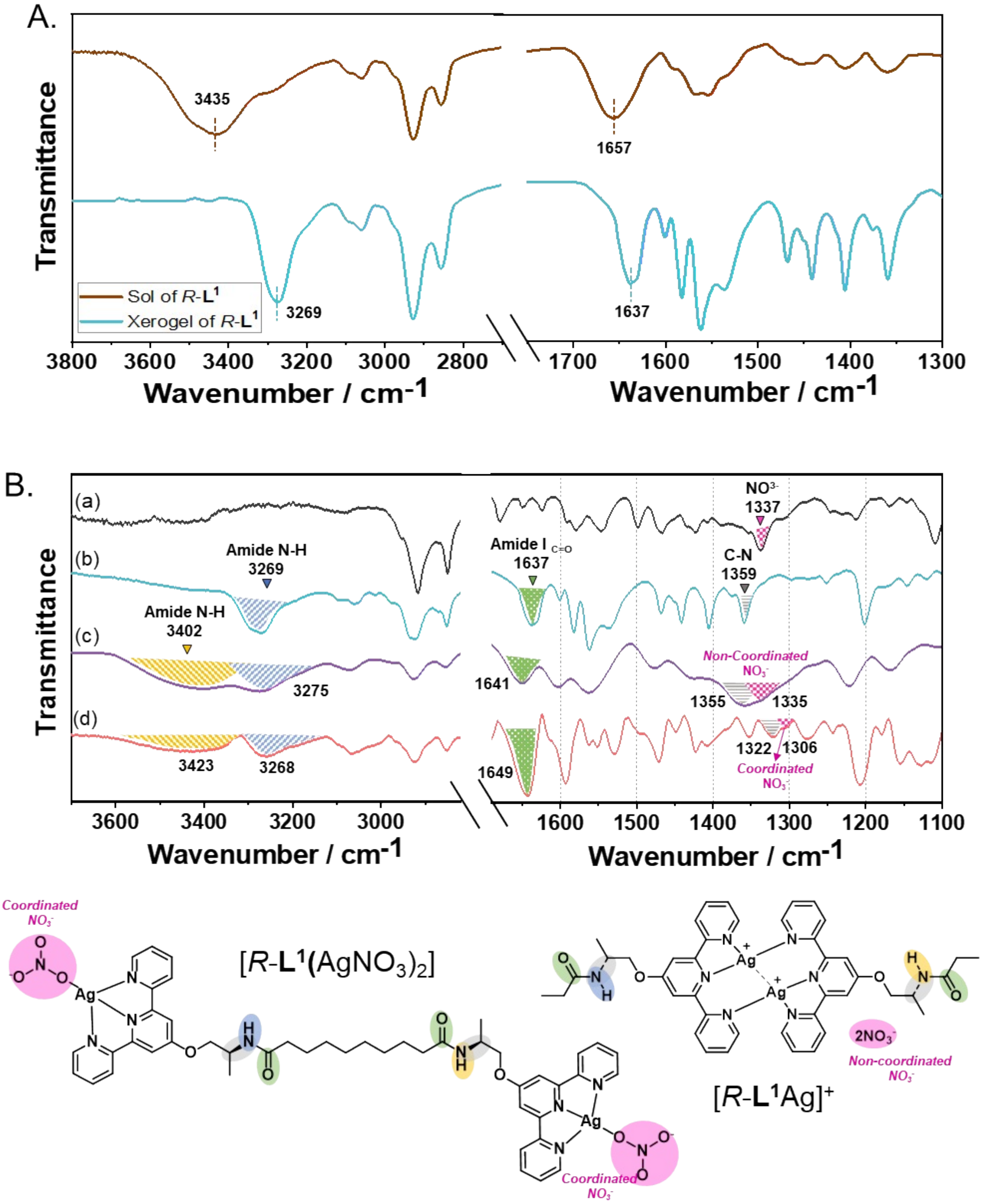

Fig. S41 (A) FT-IR spectra of sol state (brown line) of R-$\mathbf{L}^1$ and aggregate I (blue line). (B) FT-IR spectra of (a) $AgNO_3$ (black line), (b) aggregate I (blue line), (c) aggregate II (purple line), and (d) aggregate III (pink line).

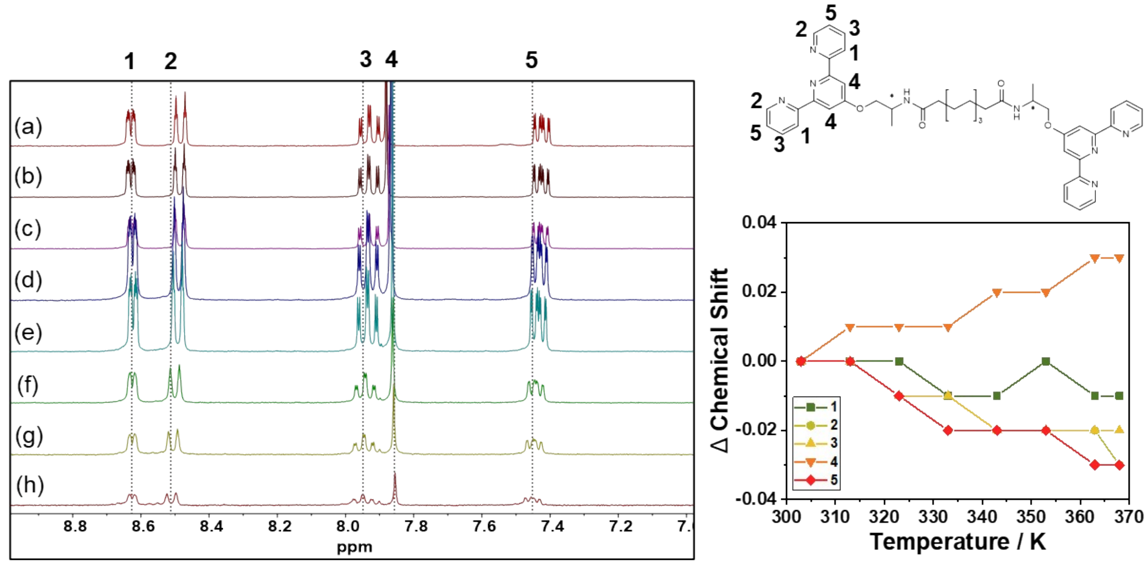

Fig. S42 Temperature-dependent ^{1}H NMR spectra of aggregate I in DMSO-d_6/D_2O (1:1 v/v); (a) 368 K, (b) 363 K, (c) 353 K, (d) 343 K, (e) 333 K, (f) 323 K, (g) 313 K, and (h) 303 K.

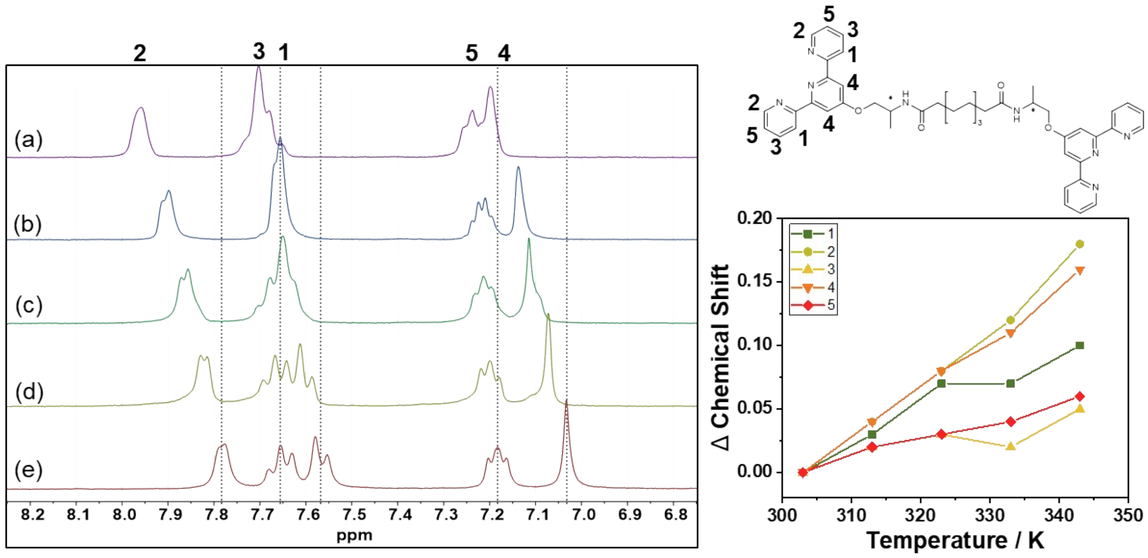

Fig. S43 Temperature-dependent ^{1}H NMR spectra of aggregate II in DMSO-d_6/D_2O (1:1 v/v); (a) 343 K, (b) 333 K, (c) 323 K, (d) 313 K, and (e) 303 K.

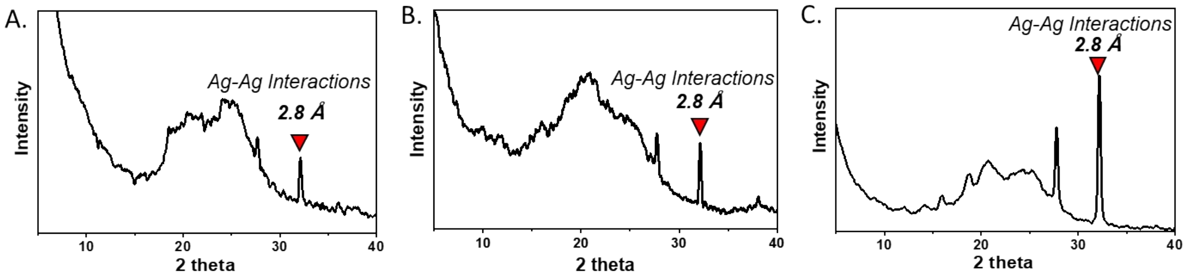

Fig. S44 WAXD patterns of *R*-**L**^{1} (6.4 mM) in the presence of different equiv. of $AgNO_3$ in DMSO/H_2O (1:1 v/v): (A) 0.5 equiv., (B) 0.8 equiv., and (C) 1.2 equiv.

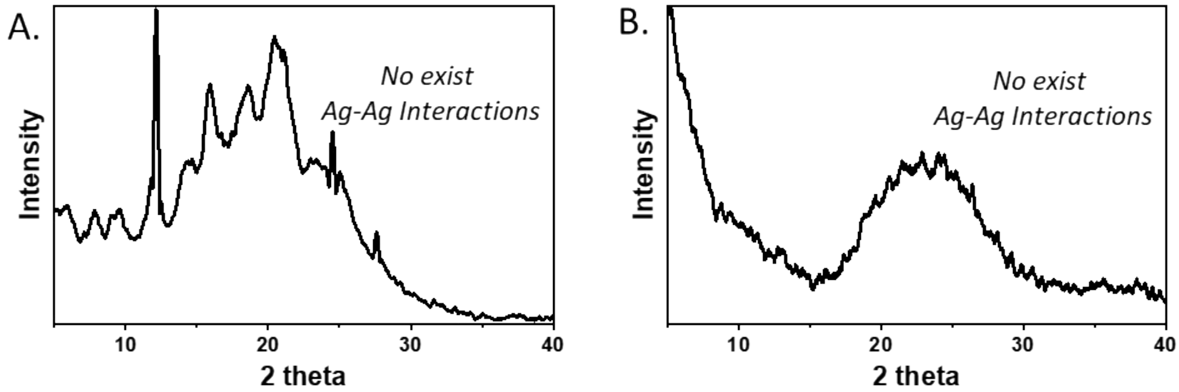

Fig. S45 WAXD patterns of *R*-**L**^{1} (6.4 mM) in the presence of different equiv. of $AgNO_3$ in DMSO/H_2O (1:1 v/v): (A) 0 equiv., (B) 2.0 equiv.

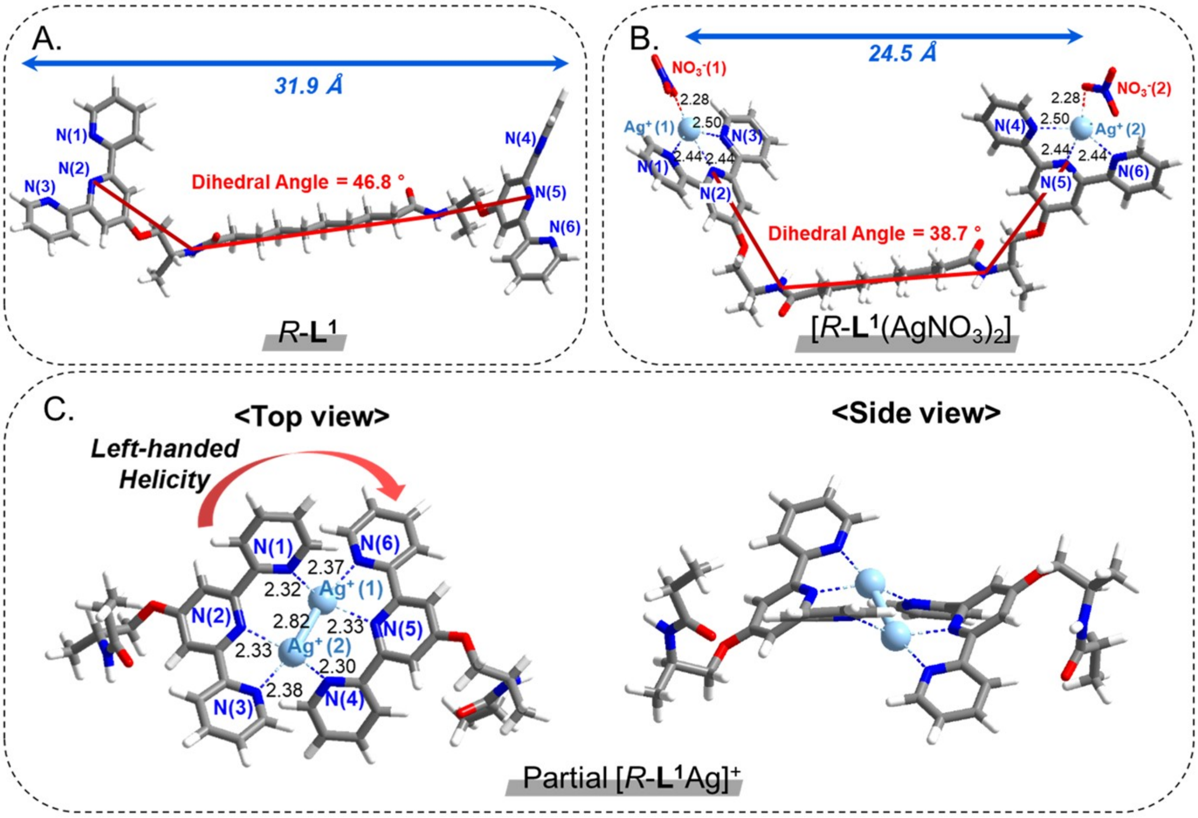

Fig. S46 DFT-optimized structures of (A) *R*-**L**¹, (B) [*R*-**L**¹(AgNO$_3$)$_2$], and (C) partial [*R*-**L**¹Ag]$^+$. Note for the structure (C): Since NO$_3^-$ remains uncoordinated in the FT-IR study, its coordination was ignored in the DFT calculation.

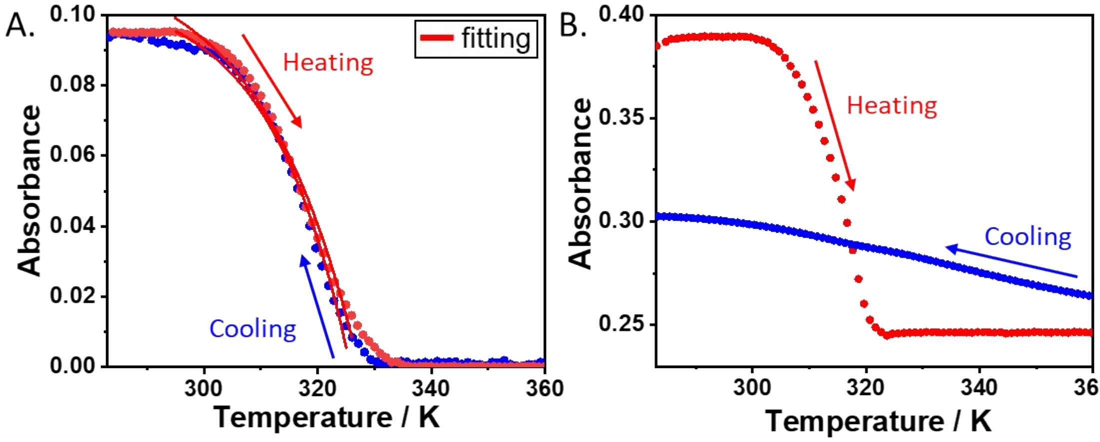

Fig. S47 Temperature-dependent absorption changes of (A) aggregate I and (B) aggregate II through heating (red points) and cooling (blue points).

[*Note*] In our repeated measurements of the cooling and heating curves for aggregate I (based on *R*-**L**¹), no evidences of the hysteresis were found (Fig. S47A). During the heating and cooling, the T_e values are 327.2 and 325.7 K, respectively. While the T_m values are 317.5 and 316.9 K, respectively.

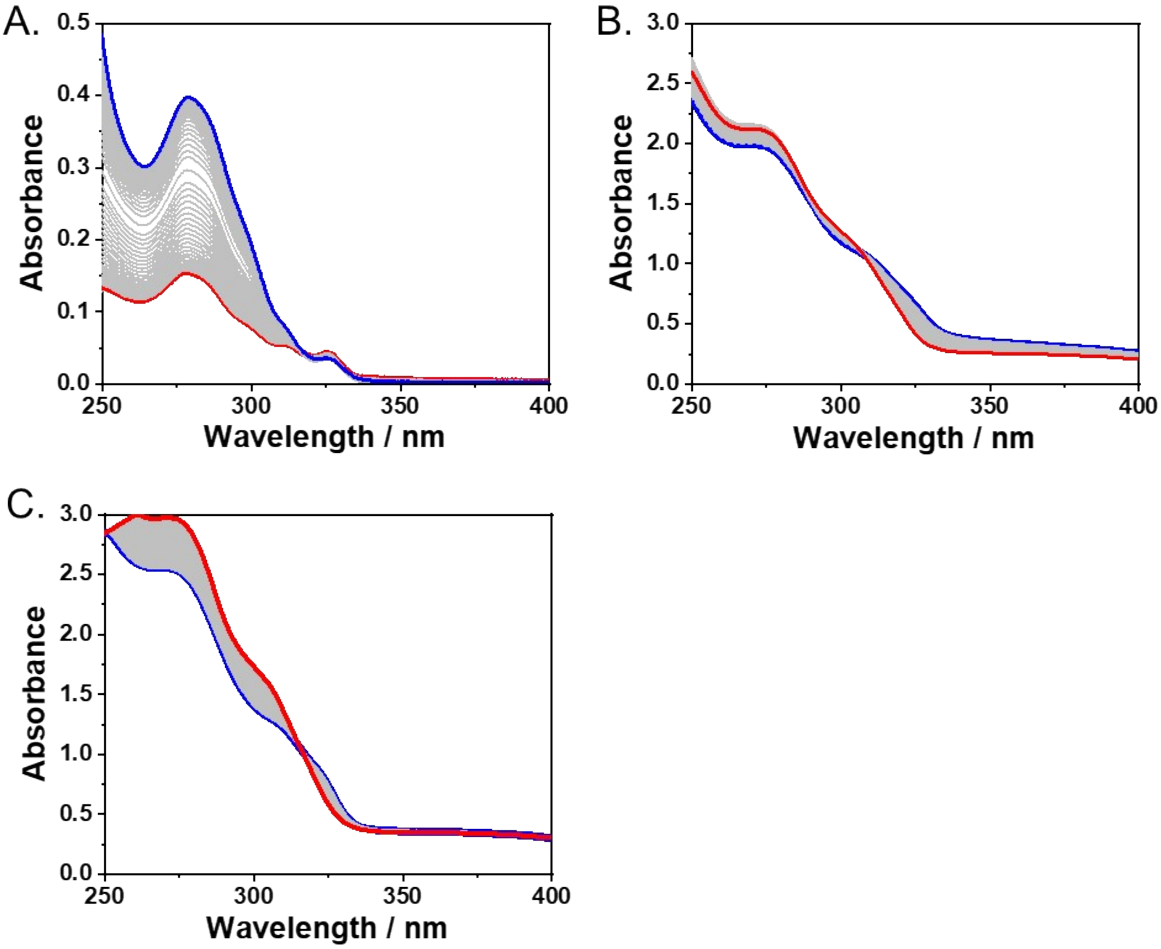

Fig. S48 Temperature-dependent UV spectra of different concentrations of *R*-**L**^{1} with $AgNO_3$ (A) aggregate I, (B) aggregate II, and (C) aggregate III in DMSO/H_2O (1:1 v/v). The melting curves of aggregate II and aggregate III were measured by varying the aging time of the same sample (1.2 equiv. of $AgNO_3$). Aggregates I and II were measured after aging for 3 days, and aggregate III was measured after aging for 1 h.

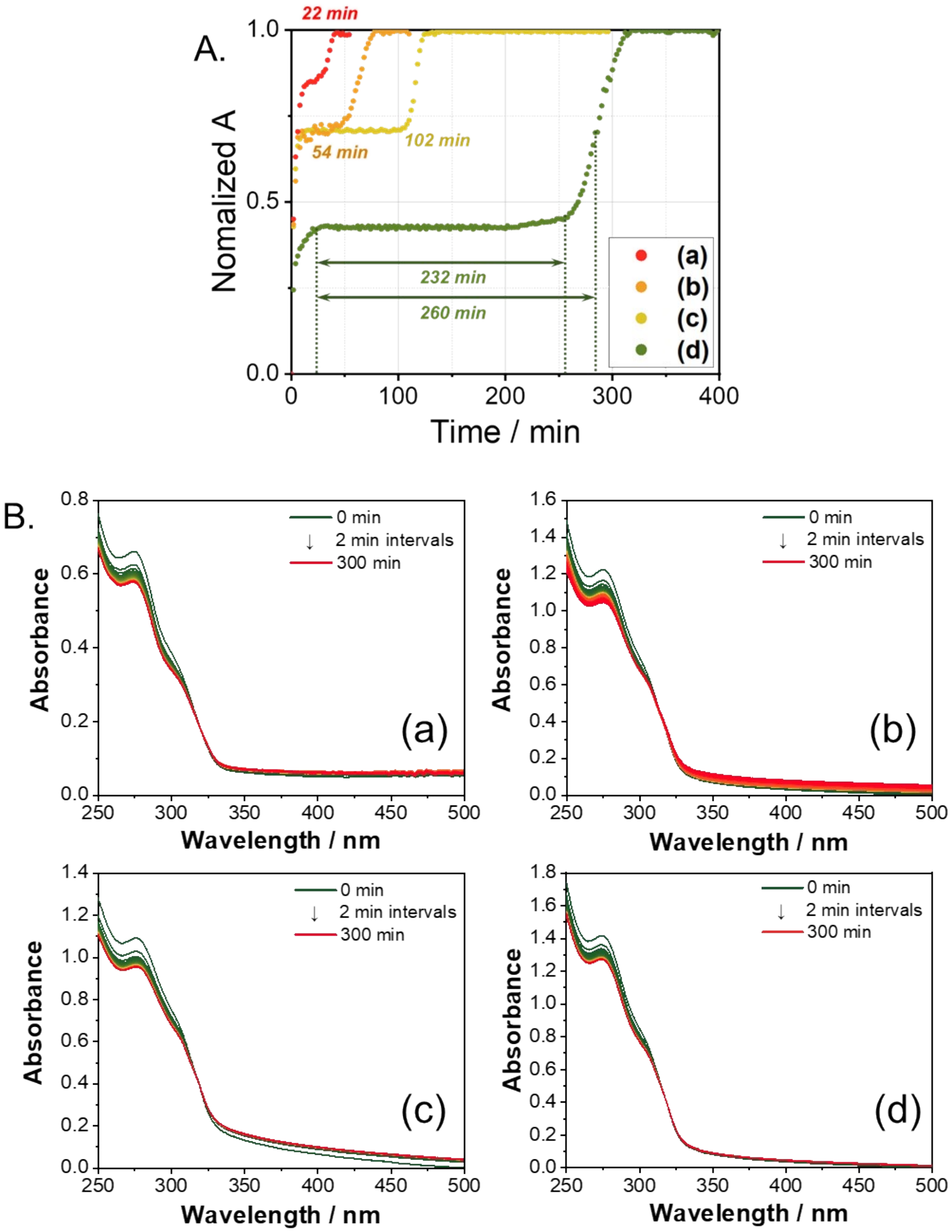

Fig. S49 (A) Time-dependent UV-vis spectral changes of different [R-$\mathbf{L}^1$] in the presence 0.6 equiv. of $AgNO_3$ in DMSO/H_2O (1:1 v/v): (a) 6.4 mM, (b) 6.8 mM, (c) 7.2 mM, and (d) 8.5 mM. (B: raw spectral data for the plots in A) Time-dependent UV-vis spectra of different [R-$\mathbf{L}^1$] in the presence 0.6 equiv. of $AgNO_3$: (a) 6.4 mM, (b) 6.8 mM, (c) 7.2 mM, and (d) 8.5 mM in DMSO/H_2O (1:1 v/v) at 20 ^{o}C (cell path length: 0.1 mm).

Table S1. Photochemical, helical, and morphology propeties of suprmolecular polymers based on *R*-$\mathbf{L}^1$ without and with $AgNO_3$.

		$[R\text{-}\mathbf{L}^1]_n$	$[R\text{-}\mathbf{L}^1\mathbf{Ag}]^+_n$	$[R\text{-}\mathbf{L}^1(\mathbf{AgNO_3})_2]_n$
UV-vis absorption	**ILCT**	280 nm	285 nm	285 nm
	MLCT	*No MLCT*	318 nm, 326 nm	318 nm, 326 nm
CD		Positive(*P*-type)	Negative(*M*-type)	Negative(*M*-type)
Morphology		Right-handed helix 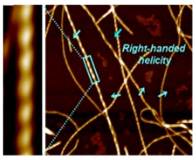 	Left-handed helix 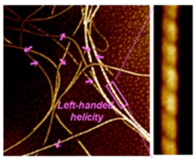 	Spherical structure 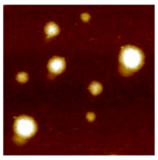
Pitch	**Angle**	*ca.* 28±3 °	*ca.* 30±3 °	
	Length	*ca.* 55±7 nm	*ca.* 75±5 nm	
Height		*ca.* 8 nm	*ca.* 5 nm	*ca.* 7.5 nm

Table S2. Cartesian coordinates of an optimized structure for *R*-$\mathbf{L}^1$.

atom	x	y	z	atom	x	y	z
O	20.34365	-6.24608	-2.00909	C	1.82848	0.18669	1.81205
O	16.88319	-3.24205	-3.47785	C	2.18332	1.46574	2.24218
O	5.37778	-5.06214	-1.13148	C	1.18736	2.43657	2.35309
O	1.13451	-4.27374	-1.0479	C	-0.12463	2.07062	2.02935
N	23.26064	-10.4009	1.05595	H	24.12196	-4.10394	0.13602
N	23.56973	-5.77757	3.02392	H	25.47902	-2.67092	1.67436
N	22.71489	-7.64564	1.09797	H	19.15803	-3.6598	-3.72442
N	17.96563	-5.21253	-3.14253	H	19.88235	-4.28622	-1.49065
N	4.21376	-4.60544	-3.02156	H	21.25165	-4.47956	-2.63137
N	-3.80583	-2.66107	1.81472	H	20.7719	-5.01773	-5.09962
N	-1.12425	-1.88857	1.49042	H	19.92074	-6.5101	-4.6324
N	-0.47187	0.85201	1.62226	H	19.08667	-5.27804	-5.62215
C	20.94845	-10.7713	0.52017	H	17.89463	-6.16864	-2.81395
C	21.07487	-12.1268	0.82529	H	4.25495	-4.2617	-3.97384
C	22.31569	-12.6073	1.24543	H	19.98504	-10.361	0.21144
C	23.37382	-11.6958	1.34215	H	20.21353	-12.7952	0.7442
C	24.29709	-5.01334	3.83548	H	22.4646	-13.6599	1.49715
C	25.00267	-3.88141	3.41019	H	24.3643	-12.037	1.66815
C	24.93682	-3.53861	2.05937	H	24.32421	-5.31286	4.89056
C	24.17316	-4.33206	1.2025	H	25.58753	-3.29241	4.1204
C	23.50013	-5.45068	1.72657	H	20.615	-8.69953	-1.3483
C	22.07255	-9.93514	0.64809	H	21.88288	-4.70055	-0.33785
C	21.98778	-8.47208	0.33498	H	15.581	-4.9599	-1.51368
C	22.67405	-6.33847	0.84489	H	15.62528	-6.17039	-2.79773
C	21.89925	-5.77909	-0.19045	H	14.29999	-4.63596	-4.29306
C	21.18443	-8.01632	-0.71715	H	14.35478	-3.38244	-3.06216

C	21.13627	-6.64108	-0.98593	H	13.04705	-4.88261	-1.48968
C	20.25481	-4.86682	-2.35268	H	12.9918	-6.13273	-2.73082
C	19.79583	-5.42824	-4.79492	H	11.73036	-4.55833	-4.25189
C	19.28525	-4.73505	-3.52646	H	11.78502	-3.3163	-3.00345
C	16.85515	-4.41132	-3.1287	H	10.48578	-4.83502	-1.44941
C	15.58367	-5.08266	-2.61319	H	10.41689	-6.05913	-2.71475
C	14.30965	-4.47472	-3.20031	H	9.15861	-4.44568	-4.19695
C	13.02588	-5.03658	-2.58487	H	9.22764	-3.22861	-2.92398
C	11.74997	-4.41086	-3.15599	H	7.91604	-4.7642	-1.38844
C	10.4597	-4.96686	-2.54689	H	7.845	-5.96922	-2.6656
C	9.18543	-4.32022	-3.09807	H	6.52556	-4.37763	-4.10406
C	7.90058	-4.88119	-2.48405	H	6.69923	-3.12101	-2.87662
C	6.63091	-4.2164	-3.01678	H	1.80367	-4.55502	-4.3097
C	5.36908	-4.67828	-2.29019	H	2.36857	-6.24567	-4.16537
C	1.96519	-5.38893	-3.60401	H	0.98696	-5.67008	-3.1912
C	2.9145	-4.98419	-2.47964	H	3.08359	-5.84056	-1.80731
C	2.36364	-3.84446	-1.61278	H	2.20836	-2.93653	-2.22669
C	-4.9895	-3.0465	2.28536	H	3.0952	-3.61575	-0.82005
C	-5.29481	-4.36859	2.62978	H	-4.48126	-6.3769	2.73626
C	-4.29839	-5.33238	2.47033	H	-2.24926	-5.6641	1.86072
C	-3.05575	-4.93723	1.97443	H	-5.74722	-2.26084	2.39729
C	-2.84718	-3.58295	1.65371	H	-6.28363	-4.62813	3.01504
C	-0.77419	-3.93091	0.27204	H	1.82145	-1.76519	-0.16419
C	-1.52908	-3.11064	1.11894	H	-1.12569	-4.91176	-0.04969
C	0.45564	-3.46002	-0.20958	H	2.58106	-0.60102	1.73955
C	0.88411	-2.1896	0.19139	H	3.22152	1.69626	2.4956
C	0.05152	-1.44387	1.04878	H	1.41467	3.45197	2.68601
C	0.48109	-0.08269	1.50836	H	-0.93451	2.80704	2.10432

Table S3. Cartesian coordinates of an optimized structure for [*R*-**L**^{1}(AgNO$_3$)$_2$].

atom	x	y	z	atom	x	y	z
Ag	-1.82356	-1.66345	3.23628	C	-1.01212	-3.29874	0.48541
Ag	22.86432	-6.93279	3.31484	C	1.00908	-3.19914	-0.8307
O	23.66205	-6.22014	5.32723	C	1.60942	-2.48651	0.21666
O	24.78481	-7.25705	6.86734	C	0.84781	-2.22313	1.3673
O	24.24329	-8.29714	5.03959	C	1.41884	-1.46418	2.52765
O	-4.14505	-0.81871	4.02301	C	2.8001	-1.39567	2.77173
O	-4.32043	-0.31223	6.12736	C	3.25661	-0.67205	3.87465
O	-2.42121	-1.00313	5.33743	C	2.32865	-0.0449	4.70736
O	20.0495	-7.09945	-2.58035	C	0.97074	-0.17474	4.39951
O	17.18979	-5.05571	-5.78945	H	21.30362	-3.09877	-0.2439
O	5.6253	-4.90053	-2.50909	H	22.43026	-1.15751	0.8373
O	1.61313	-3.50397	-1.99266	H	19.41316	-5.59775	-5.47641
N	24.2482	-7.27334	5.77304	H	19.5613	-5.14423	-3.09624
N	-3.65974	-0.70043	5.17906	H	21.14635	-5.73041	-3.69961
N	21.87497	-9.09177	2.76091	H	21.20617	-7.35789	-5.69711
N	23.0669	-4.75383	2.11528	H	20.17326	-8.52404	-4.83692

N	21.55054	-6.85497	1.25045	H	19.67095	-7.89132	-6.43016
N	18.02277	-6.78249	-4.5694	H	17.80904	-7.5678	-3.96603
N	4.77561	-3.28406	-3.84921	H	4.97839	-2.51329	-4.47468
N	-3.11124	-2.98592	1.63649	H	19.52437	-10.3557	0.69223
N	-0.41966	-2.62476	1.48306	H	19.70895	-12.2571	2.29098
N	0.53862	-0.85712	3.33805	H	21.33148	-12.0837	4.21496
C	20.22956	-10.3045	1.52265	H	22.69257	-9.955	4.44223
C	20.32898	-11.3668	2.423	H	24.28637	-3.9521	3.57363
C	21.22194	-11.2734	3.4914	H	23.96746	-1.57456	2.79539
C	21.97818	-10.1041	3.62463	H	20.07633	-9.00497	-0.90412
C	23.65348	-3.71514	2.71186	H	21.22677	-4.89125	-1.47064
C	23.46615	-2.39758	2.28225	H	15.61197	-7.21192	-3.89387
C	22.61812	-2.17213	1.19716	H	15.29824	-7.2012	-5.63223
C	21.9959	-3.26061	0.58347	H	14.6567	-4.76326	-5.48965
C	22.24886	-4.55305	1.07099	H	14.85616	-4.81356	-3.74187
C	21.03279	-9.17036	1.72072	H	13.07183	-6.60378	-3.58409
C	21.01525	-7.99517	0.78874	H	12.85948	-6.53567	-5.33272
C	21.61712	-5.77389	0.47108	H	12.18601	-4.11259	-5.15674
C	21.1279	-5.77613	-0.84631	H	12.40017	-4.17757	-3.40908
C	20.49502	-8.08222	-0.50415	H	10.60667	-5.94273	-3.24936
C	20.54955	-6.95397	-1.33898	H	10.39467	-5.88848	-4.99795
C	20.09621	-6.01626	-3.50984	H	9.71989	-3.46827	-4.8477
C	20.16104	-7.63064	-5.48075	H	9.94902	-3.50668	-3.10048
C	19.42351	-6.47	-4.80485	H	8.14303	-5.25443	-2.88484
C	16.9969	-6.04179	-5.09687	H	7.93119	-5.25701	-4.63283
C	15.59546	-6.55793	-4.7831	H	7.18148	-2.86047	-4.55714
C	14.57606	-5.42936	-4.61551	H	7.52989	-2.80075	-2.82538
C	13.13661	-5.9235	-4.45412	H	2.56258	-2.03557	-4.85326
C	12.11988	-4.79066	-4.28579	H	2.80751	-3.58976	-5.70263
C	10.67469	-5.27052	-4.12467	H	1.45	-3.39243	-4.56204
C	9.66139	-4.13327	-3.96553	H	3.3247	-4.72842	-3.53972
C	8.22127	-4.61693	-3.78036	H	3.01121	-1.97987	-2.2281
C	7.21059	-3.47574	-3.64124	H	3.62615	-3.48915	-1.46598
C	5.81379	-3.97039	-3.27732	H	-4.96752	-5.67385	-0.42777
C	2.5008	-3.13302	-4.74927	H	-2.55076	-5.22148	-0.83144
C	3.38081	-3.62969	-3.60569	H	-4.86417	-2.62005	2.6531
C	2.95125	-3.08453	-2.23768	H	-6.18007	-4.34909	1.34438
C	-4.40494	-3.22376	1.86217	H	2.62981	-2.11921	0.13601
C	-5.12186	-4.18012	1.13538	H	-0.79683	-4.14063	-1.51762
C	-4.44821	-4.90726	0.15282	H	3.50881	-1.92169	2.13047
C	-3.09583	-4.6501	-0.07908	H	4.32688	-0.61183	4.0873
C	-2.45241	-3.66486	0.6864	H	2.64246	0.52533	5.58395
C	-0.32585	-3.61303	-0.68902	H	0.19469	0.2716	5.03033

Table S4. Cartesian coordinates of an optimized Structure for Partial [*R*-**L**^{1}Ag]$^+$.

atom	x	y	z	atom	x	y	z
Ag	3.15211	-1.25144	0.8467	C	10.45429	1.68764	-0.06042
Ag	3.58523	1.47762	1.45262	C	11.46025	2.55669	0.71412

O	-3.38266	1.31004	-0.8902	C	12.45217	3.20841	-0.25491
O	-2.9963	-0.93771	1.73704	C	10.41521	3.54984	2.83587
O	9.70799	0.79438	0.78368	C	11.06207	2.51053	3.74266
O	9.59967	4.3631	3.25108	C	10.64339	2.65922	5.20228
N	2.29449	-3.44141	0.48382	H	8.29636	3.16137	0.91461
N	-4.9286	-0.27001	-0.34558	H	8.3027	-1.05934	1.7876
N	0.89195	-1.0259	0.3258	H	-1.59251	-3.02439	1.48502
N	2.10177	1.64182	-0.29999	H	-1.59432	1.21538	0.74719
N	4.46445	3.6604	1.76068	H	3.0187	-2.77934	3.18868
N	5.8083	1.21141	2.10738	H	4.06318	-4.50345	0.27049
N	4.57955	-1.51131	2.65756	H	6.55903	-3.06399	5.6274
N	10.78145	3.56743	1.51174	H	7.56845	-1.27439	4.20485
C	0.94692	-5.83956	0.09141	H	4.1924	-3.80793	5.11777
C	2.34199	-5.80556	0.07322	H	3.65989	2.83781	-0.98752
C	2.9715	-4.57696	0.27514	H	2.30781	4.02725	-2.69555
C	0.24165	-4.65514	0.30713	H	-0.16032	3.48222	-2.87183
C	0.94922	-3.45871	0.50403	H	-5.56936	-0.95232	-0.73526
C	-3.25919	0.49714	-3.62149	H	-0.84803	-4.66144	0.29337
C	-4.38539	0.04747	-2.69756	H	-2.30499	0.01372	-3.35825
C	-4.17125	0.43147	-1.23578	H	-3.49089	0.24079	-4.66557
C	-6.02366	1.28859	1.26452	H	-3.11675	1.58568	-3.55863
C	-5.13786	0.04993	1.0702	H	-4.5477	-1.04164	-2.77019
C	-3.8379	0.21835	1.86659	H	-5.33849	0.51307	-3.00901
C	-1.09086	0.25512	0.79819	H	-5.6556	-0.82841	1.48766
C	-1.75931	-0.8939	1.25344	H	-5.54552	2.18163	0.83421
C	-1.07324	-2.12096	1.16767	H	-6.99531	1.14528	0.76976
C	0.2368	-2.15231	0.69402	H	-6.21654	1.47507	2.33256
C	0.21498	0.13724	0.31758	H	-4.09296	0.29712	2.9342
C	2.60255	2.59367	-1.1138	H	-3.31971	1.13024	1.55702
C	1.84126	3.27129	-2.06153	H	0.40969	-6.77677	-0.07119
C	0.80245	1.30128	-0.42567	H	2.93374	-6.70655	-0.09779
C	-0.03945	1.96871	-1.33486	H	-1.09502	1.69388	-1.40854
C	0.4841	2.9652	-2.1571	H	2.721	4.78272	1.82233
C	6.48559	2.31074	1.71296	H	3.88081	6.91949	2.41803
C	6.46983	0.03839	2.17957	H	6.38799	6.88216	2.71452
C	7.78372	-0.10154	1.73901	H	7.61303	4.73536	2.41255
C	7.79772	2.2502	1.23089	H	9.76849	2.31409	-0.65503
C	8.46354	1.01405	1.21032	H	10.99459	1.02389	-0.75077
C	3.80808	4.81186	1.94336	H	13.00602	2.45147	-0.82991
C	5.80415	3.63359	1.88798	H	11.93636	3.86803	-0.97322
C	6.53431	4.78058	2.23505	H	13.178	3.81757	0.30197
C	4.45648	6.00333	2.27394	H	12.01335	1.89266	1.39392
C	5.84277	5.97943	2.42913	H	10.40543	4.36691	1.006
C	4.0325	-2.4616	3.44206	H	12.15812	2.59537	3.63893
C	5.82943	-1.08954	2.93326	H	10.80908	1.50468	3.36306
C	6.56512	-1.64585	3.99385	H	9.55336	2.56393	5.31476
C	4.69421	-3.04651	4.51819	H	11.12886	1.89061	5.82159
C	5.99718	-2.63473	4.79462	H	10.92384	3.64688	5.59505

Table S5. Thermodynamic parameters for aggregate I, aggregate II, and aggregate III (*R*-**L**^{1}: 7 mM) in mixed DMSO and H_2O (1:1 v/v).

	Δ*G* (kJ mol$^{–1}$)	**Δ*H*$_e$ (kJ mol$^{–1}$)**	**Δ*S* (J K$^{–1}$ mol$^{–1}$)**	***K*$_e$ (L mol$^{–1}$)**	***T*$_e$ (K)**
Aggregate I	-22.25	–89.6	–226	1.4×10^4	335.70
Aggregate II	-20.33	-155.22	-453	1.0×10^4	314.28
Aggregate III	-17.48	-171.81	-518	3.7×10^3	307.28

[a]Gibbs free energy. [b]Elongation enthalpy. [c]Entropy. [d]Elongation binding constant. [e]Elongation Temperature. The melting curves of aggregate II and aggregate III were measured by varying the aging time of the same sample ($AgNO_3$ 1.2 equiv.). Aggregates I and II were measured after aging for 3 days, and aggregate III was measured after aging for 1 hour.

4. Analytical data

4.1 ^{1}H-NMR and ^{13}C-NMR spectoscopy

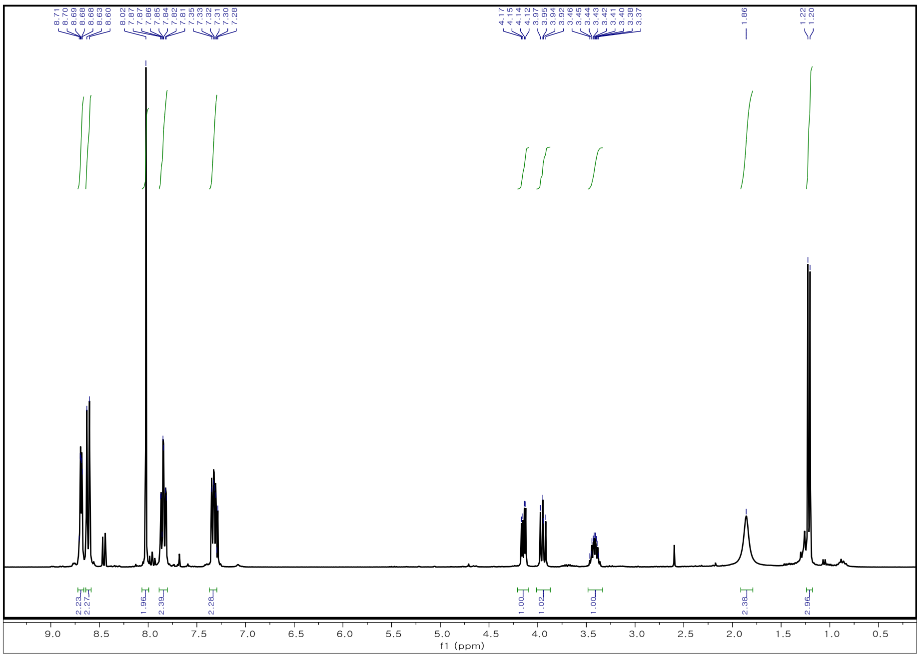

Fig. S51 ^{1}H NMR spectrum (300 MHz) of *R*-**L**^{2} in CDCl$_3$ at 25 °C.

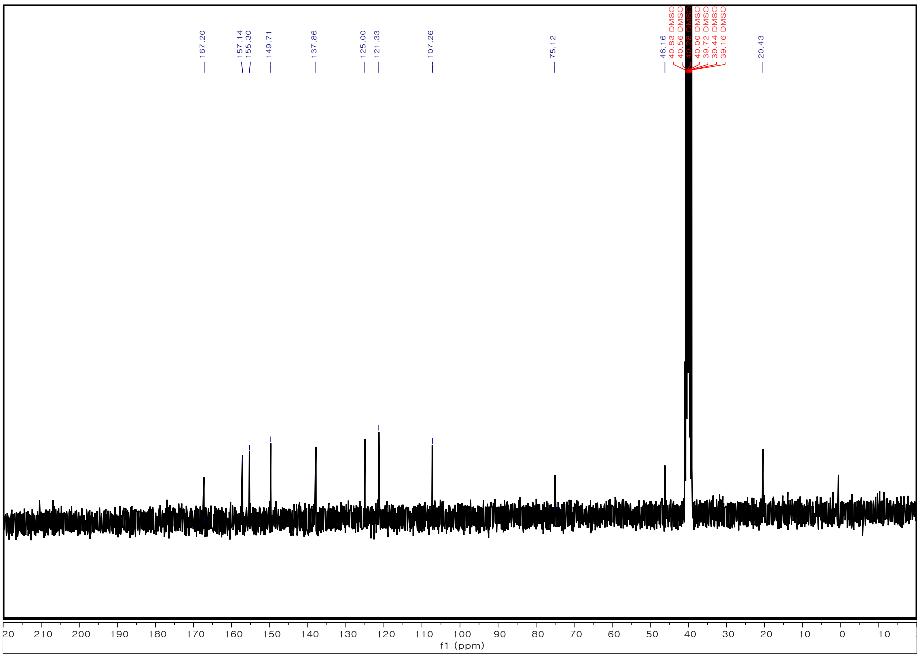

Fig. S52 ^{13}C NMR spectrum (75 MHz) of *R*-**L**^{2} in DMSO-d_6 at 25 °C.

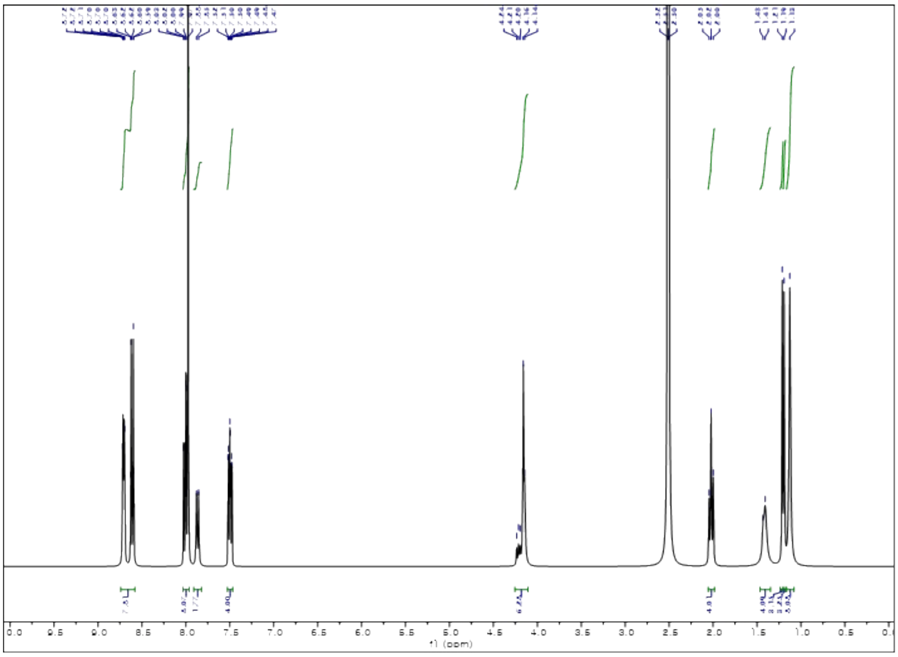

Fig. S53 ^{1}H NMR spectrum (300 MHz) of *R*-**L^1** in DMSO-d_6 at 25 °C.

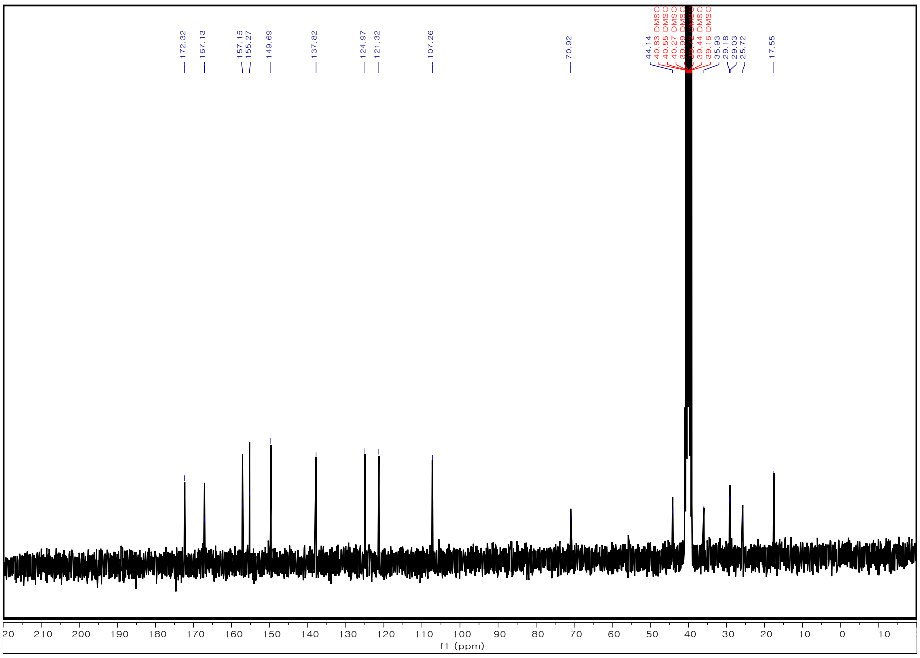

Fig. S54 ^{13}C NMR spectrum (75 MHz) of *R*-**L^1** in DMSO-d_6 at 25 °C.

4.2 HR mass spectrometry

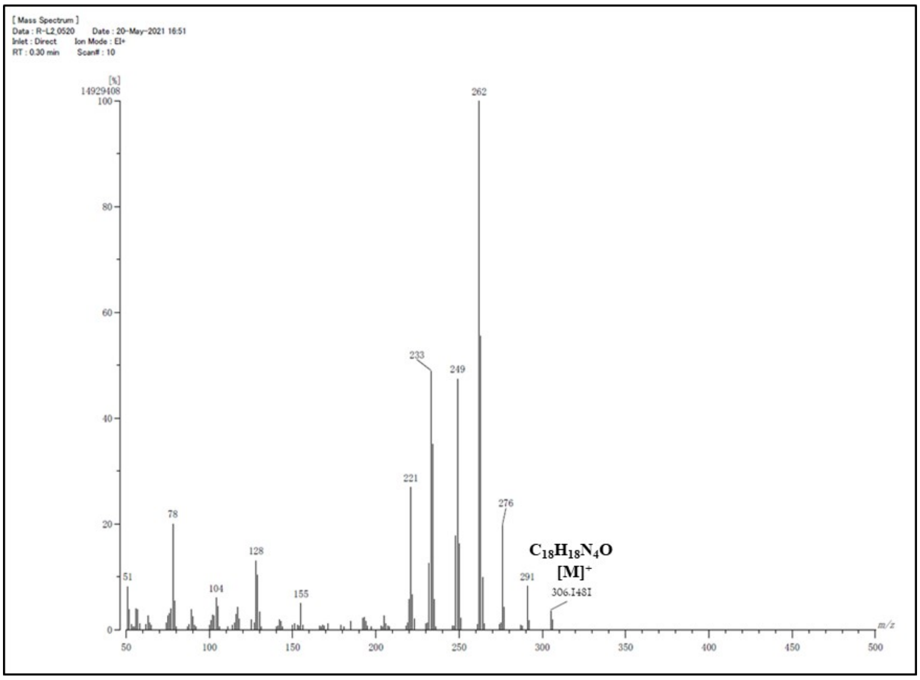

Fig. S55 HR EI-MS spectrum of *R*-$\mathbf{L}^2$ in DCM.

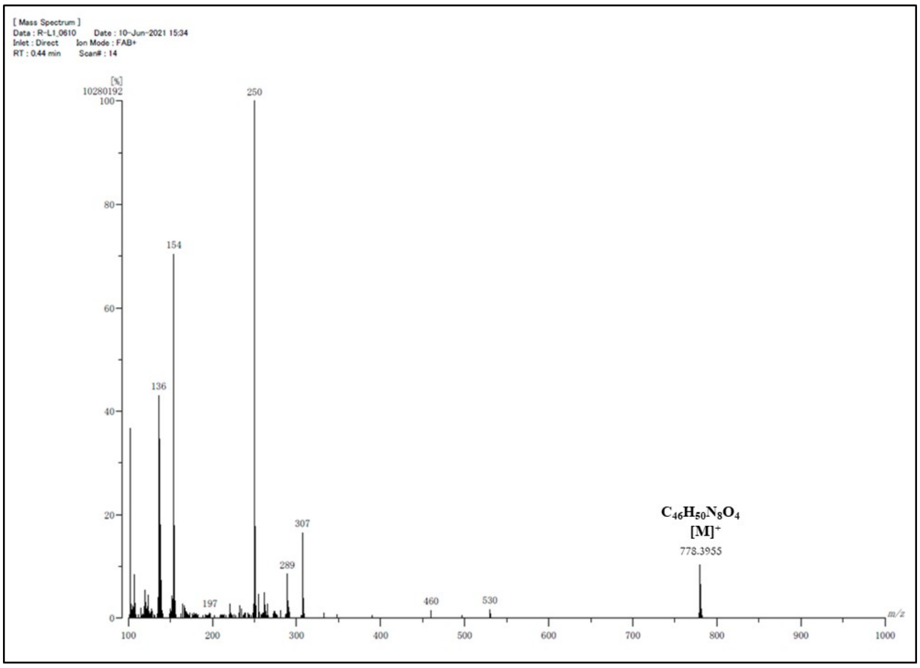

Fig. S56 HR FAB-MS spectrum of *R*-$\mathbf{L}^1$ in DCM.

5. Supplementary references

1 H. M. M. ten Eikelder, A. J. Markvoort, T. F. A. de Greef and P. A. J. Hilbers, *J. Phys. Chem. B*, 2012, **116**, 5291-5301.

2 M. M. J. Smulders, M. M. L. Nieuwenhuizen, T. F. A. de Greef, P. van der Schoot, A. P. H. J. Schenning and E. W. Meijer, *Chem. Eur. J.*, 2010, **16**, 362-367.

3 H. Choi, S. Ogi, N. Ando and S. Yamaguchi, *J. Am. Chem. Soc.*, 2021, **143**, 2953-2961.

4 M. H.-Y. Chan, M. Ng, S. Y.-L. Leung, W. H. Lam and V. W.-W. Yam, *J. Am. Chem. Soc.*, 2017, **139**, 8639-8645.

5 http://www.hyperquad.co.uk/HypSpec2014.htm.

6 P. Gans, A. Sabatini and A. Vacca, *Talanta*, 1996, **43**, 1739-1753.

7 H. Ju, T. Abe, Y. Takahashi, Y. Tsuruoka, A. Otsuka, E. Lee, M. Ikeda, S. Kuwahara and Y. Habata, *Inorg. Chem.*, 2021, **60**, 1738-1745.

8 G. W. T. M. J. Frisch, H. B. Schlegel, G. E. Scuseria, M. A. Robb, J. R. Cheeseman, G. Scalmani, V. Barone, B. Mennucci, G. A. Petersson, H. Nakatsuji, M. Caricato, X. Li, H. P. Hratchian, A. F. Izmaylov, J. Bloino, G. Zheng, J. L. Sonnenberg, M. Hada, M. Ehara, K. Toyota, R. Fukuda, J. Hasegawa, M. Ishida, T. Nakajima, Y. Honda, O. Kitao, H. Nakai, T. Vreven, J. A. Montgomery, Jr., J. E. Peralta, F. Ogliaro, M. Bearpark, J. J. Heyd, E. Brothers, K. N. Kudin, V. N. Staroverov, R. Kobayashi, J. Normand, K. Raghavachari, A. Rendell, J. C. Burant, S. S. Iyengar, J. Tomasi, M. Cossi, N. Rega, J. M. Millam, M. Klene, J. E. Knox, J. B. Cross, V. Bakken, C. Adamo, J. Jaramillo, R. Gomperts, R. E. Stratmann, O. Yazyev, A. J. Austin, R. Cammi, C. Pomelli, J. W. Ochterski, R. L. Martin, K. Morokuma, V. G. Zakrzewski, G. A. Voth, P. Salvador, J. J. Dannenberg, S. Dapprich, A. D. Daniels, Ö. Farkas, J. B. Foresman, J. V. Ortiz, J. Cioslowski, and D. J. Fox, *Journal*, 2009.

9 J. P. Perdew, *Phys. Rev. B*, 1986, **33**, 8822-8824.

10 F. Weigend, *Phys. Chem. Chem. Phys.*, 2006, **8**, 1057-1065.

11 F. Weigend and R. Ahlrichs, *Phys. Chem. Chem. Phys.*, 2005, **7**, 3297-3305.

12 C. Kim, K. Y. Kim, J. H. Lee, J. Ahn, K. Sakurai, S. S. Lee and J. H. Jung, *ACS Appl. Mater. Interfaces*, 2017, **9**, 3799-3807.